Time-Resolved Rhodopsin Activation Currents in a Unicellular Expression System

Jack M. Sullivan*# and Pragati Shukla*
Departments of *Ophthalmology and #Biochemistry, State University of New York, Health Science Center at Syracuse, Syracuse, New York 13210 USA

ABSTRACT The early receptor current (ERC) is the charge redistribution occurring in plasma membrane rhodopsin during light activation of photoreceptors. Both the molecular mechanism of the ERC and its relationship to rhodopsin conformational activation are unknown. To investigate whether the ERC could be a time-resolved assay of rhodopsin structure-function relationships, the distinct sensitivity of modern electrophysiological tools was employed to test for flash-activated ERC signals in cells stably expressing normal human rod opsin after regeneration with 11-*cis*-retinal. ERCs are similar in waveform and kinetics to those found in photoreceptors. The action spectrum of the major R_2 charge motion is consistent with a rhodopsin photopigment. The R_1 phase is not kinetically resolvable and the R_2 phase, which overlaps metarhodopsin-II formation, has a rapid risetime and complex multiexponential decay. These experiments demonstrate, for the first time, kinetically resolved electrical state transitions during activation of expressed visual pigment in a unicellular environment (single or fused giant cells) containing only 6×10^6-8×10^7 molecules of rhodopsin. This method improves measurement sensitivity 7 to 8 orders of magnitude compared to other time-resolved techniques applied to rhodopsin to study the role particular amino acids play in conformational activation and the forces that govern those transitions.

INTRODUCTION

Rhodopsin is the best-characterized member of the family of heptahelical G-protein-coupled receptors (Baldwin, 1993); 11-*cis*-retinal forms a chromophore in a pocket of the protein by covalently attaching to a lysine of the seventh α-helix (Bownds, 1967). Light absorption by the chromophore promotes isomerization and charge separation in the pocket on a femtosecond time scale (Birge et al., 1988). Spectroscopic studies identified several spectral states reflecting changes in the chromophore environment on the picosecond to millisecond time scale after photon absorption (Lewis and Kliger, 1992). The metarhodopsin-II spectral state (Meta-II_{380}), which appears after a millisecond, correlates with the bulk conformational activation of rhodopsin to the R* state. In this state rhodopsin binds and activates transducin to trigger the signal amplification cascade in the rod or cone photoreceptor (Parkes and Liebman, 1984; Kibelbek et al., 1991). Structure-function studies have shown that three interhelical loops cooperate to form the transducin binding domain on the cytoplasmic face of rhodopsin during Meta-II formation (Konig et al., 1989; Farahbakhsh et al., 1995). Identifying the molecular mechanism to reach the R* conformational state remains an important problem in visual science.

Two charge-transfer events are required to achieve the R* state. The reciprocal deprotonation of the cationic Schiff base and the protonation of its anionic counterion (glutamate-113: E113) occurs first. This is followed by the net vectorial uptake of protons into the cytoplasmic face of the protein from the membrane boundary solution. Several amino acids in the intramembrane α-helices have protonatable side chains that could potentially contribute to electrically active and biochemically important processes of intramolecular proton transfer or proton uptake from solution, including D83, E113, E122, E134, H211, and Y268. Some of these have been shown to be important for transducin activation by site-directed mutagenesis (Zhukovsky and Oprian, 1989; Sakmar et al., 1989; Nathans et al., 1990a, b; Weitz and Nathans, 1992, 1993). Being remote from chromophore environment, any conformational changes on or near the cytoplasmic face of rhodopsin that are critical to R* formation are likely to be spectrally silent to absorption. Other biophysical techniques not dependent upon retinal absorption have been used to study conformation changes leading to the R* state. FTIR spectroscopic difference methods have shown conformational changes in the α-helical backbone and environmental changes at specific intramembrane side chains (e.g., D83, E122, H211) or shifts in protonation states of intramembrane carboxyl groups during the transitions between the ground state and Meta-II (Rothschild and deGrip, 1986; Ganter et al., 1988, 1989; Klinger and Braiman, 1992; Fahmy et al., 1993; Rath et al., 1993; Jager et al., 1994). Time-resolved FTIR has not been re-

Received for publication 23 September 1998 and in final form 2 June 1999.

Address reprint requests to Jack M. Sullivan, M.D. Ph.D., Assistant Professor of Ophthalmology and Biochemistry, SUNY Health Science Center, Dept. of Biochemistry, Weiskotten Hall, 4255, 750 East Adams St., Syracuse, NY 13210. Tel.: 315-464-6694; Fax: 315-464-8750; E-mail: Sullivaj@vax.cs.hscsyr.edu.

Abbreviations used: FTIR, Fourier transform infrared spectroscopy; C_{mem}, membrane capacitance; DM, *n*-dodecyl-β-D-maltopyranoside; ERC, early receptor current; ERP, early receptor potential; ESR, electron spin resonance spectroscopy; fC, femtocoulomb; PBS, phosphate buffered saline; pA, picoampere; pC, picocoulomb; pg, picogram; R_{ser}, series resistance; SD, standard deviation; SE, standard deviation of the mean; SNR, signal-to-noise ratio; WT, wild type. Single-letter chemical abbreviations are used for amino acids (e.g., D, aspartate; E, glutamate; H, histidine; K, lysine; Y, tyrosine).

0006-3495/99/09/1333/25 $2.00

ported on an expressed vertebrate visual pigment because of technical limitations in producing large quantities of an expressed mutant visual pigment for a technique with relatively low sensitivity. To better understand the role of particular amino acids in *rapid* activation processes, recent efforts have applied other time-resolved techniques to native rhodopsin or expressed mutant bovine visual pigments. These have included ESR spectroscopy (Farahbakhsh et al., 1993, 1995), rapid proton exchange (Arnis and Hofmann, 1993; Arnis et al., 1994) and more recently time-resolved absorption studies (Jager et al., 1997). These techniques require hundreds of micrograms (e.g., ESR, proton exchange) and typically tens of milligrams (e.g., absorption) of expressed and purified visual pigments solubilized away from their native membrane environments into detergents. Recent time-resolved ESR studies have demonstrated millisecond-order relative vectorial motions in α-helix III and VI during Meta-II formation (Farahbakhsh et al., 1993, 1995). The E134 side chain, which is located at the cytoplasmic end of α-helix III, is known to be essential to trigger the rapid proton uptake process as measured with pH-sensitive dyes (Fahmy and Sakmar, 1993; Arnis et al., 1994; Han et al., 1996). While informative, the limits of sensitivity of these assays require extensive effort to express (usually transiently) and purify large quantities of visual pigment for experimental analysis.

In addition to spectral states, rhodopsin has charge states identified as "conformational-dependent currents" (Honig et al., 1986). The ERP reflects the "charge redistribution" in rhodopsin during its activation (Cone, 1967; Cone and Pak, 1971; Hodgkin and O'Bryan, 1977). The signal has a broad temporal range extending from picoseconds through milliseconds. The charge motion underlying the ERP is the ERC (Hestrin and Korenbrot, 1990; Makino et al., 1991). The ERC is the net vectorial charge transfer within activated rhodopsin molecules oriented in the plasma membrane. Models of the nature of this interesting signal have been proposed including oxidation/reduction of rhodopsin (Arden et al., 1968), Schiff base deprotonation (Spalink and Stieve, 1980; Trissl, 1982b), and proton uptake (Cafiso and Hubbell, 1980). These early studies preceded the structure/function investigations of similar conformation-dependent gating currents in ionic channels during the last decade. The ERC signal is orthogonal to the membrane plane and, therefore, is sensitive to conformational and chemical changes in rhodopsin directed *across* the membrane dielectric. Molecular events that could underlie the ERC include charge separation, dipole reorientation, intramolecular proton transfer, α-helical movement, and interfacial proton (or ion) transfer. Such processes have been shown to occur during the activation of rhodopsin, but not by electrical methods (Ostroy, 1974; Bennett, 1980a, b; Parkes and Liebman, 1984; Lewis and Kliger, 1992; Farahbakhsh et al., 1993, 1995; Arnis and Hofmann, 1993). Thus, the ERC could be used as a time-resolved assay of these and similar electrical events.

The waveform of the ERC/ERP demonstrates electrical complexity over a broad temporal range. Photon absorption by 11-*cis*-retinal leads to isomerization and charge separation on a femtosecond-picosecond time scale during bathorhodopsin formation (Birge et al., 1988). This early charge redistribution in rhodopsin may underlie the brief depolarizing phase of the ERP or inward-directed R_1 current of the ERC (Trissl, 1982a). Given the similarity of the signal shape and kinetics of the photoreceptor ERP to the photovoltage of bacteriorhodopsin, a light-dependent proton pump, the R_1 phase of the photoreceptor ERP/ERC may reflect the charge separation that occurs in the retinal binding pocket when the protonated Schiff base moves relative to its counterion during isomerization (Trissl, 1982a; Simmeth and Rayfield, 1990). However, the R_1 phase of bacteriorhodopsin has the same kinetics and polarity whether or not the isomerization occurs in separate directions with different retinal analogs (Trissl and Gartner, 1987). Rhodopsin appears to be electrically silent between bathorhodopsin and metarhodopsin-I in the forward bleaching pathway (Arden et al., 1968; Ebrey, 1968; Spalink and Stieve, 1980; Drachev et al., 1981; Trissl, 1982a, b). However, when particular spectral states (Meta-I, Meta-II, Meta-III) are trapped and then photolyzed within their respective absorption bands, unique state-dependent ERP signals occur (Cone and Pak, 1971) that probably reflect charge motions associated with photoreversal (Williams, 1964). ERC components reflective of photoreversal have not yet been found in photoreceptors (Makino et al., 1991). Ebrey (1968) elegantly used the state-dependent signal property of the ERP to study the lifetimes of the Meta-I and Meta-II spectral states in the intact eye of the rat, and correlation between electrical and spectral states is established (Cone, 1967; Spalink and Stieve, 1980; Trissl, 1982b). On the millisecond time scale the R_2 phase of the ERP/ERC overlaps with metarhodopsin-I decay and Meta-II formation (Spalink and Stieve, 1980). The activation energy of Meta-II formation is similar to that of ERP R_2, suggesting related processes initiated by the essential Schiff base deprotonation and intramolecular charge transfer (Cone and Pak, 1971; Longstaff et al., 1986; Jager et al., 1994). The ERP R_2 kinetics could not be fit by models with a few discrete states, and power laws were required (Lindau and Ruppel, 1983). This suggested that formation of Meta-II generates a set of electrically active conformational/chemical states with similar activation energies and was supported by more recent spectroscopic studies of the metarhodopsin intermediates (Thorgeirsson et al., 1993; Arnis and Hofmann, 1993). Cafiso and Hubbell (1980) elegantly demonstrated that Meta-II formation leads to a transient positive electrical perturbation within the rod disk membrane dielectric near its cytoplasmic face when assayed with potential-sensitive ESR probes. This intramembrane depolarization (with respect to the cytoplasm) correlated with the temporal appearance of Meta-II and was titratable by cytoplasmic pH ($pK_a \approx 6.8$) in a manner consistent with the pH-sensitivity of the Meta-I/Meta-II equilibrium (Parkes and Liebman, 1984). They

suggested that this electrodynamic potential was related to the R_2 phase of the ERP and reflected the proton uptake into rhodopsin during R* formation. However, Spalink and Stieve (1980), Bennett (1980b), and Lindau and Ruppel (1985) proposed that a significant component of the ERP originated from intramolecular charge transfer associated with Schiff base deprotonation and was independent of proton uptake. These studies suggested the ERP could be a useful assay to monitor Schiff base deprotonation and proton uptake processes associated with R* formation during the Meta-II lifetime. Moreover, a combination of site-specific mutagenesis and electrical measurements should allow hypotheses about the molecular transitions underlying the R_2 to be put to experimental test.

The remaining challenges to understand the molecular mechanism underlying R* formation led to consideration whether the sensitivity and time-resolution of gigaohm-seal electrophysiological techniques could be applied to structure/function problems in expressed visual pigments. Gigaohm-seal whole-cell recording had been used to study ERCs in rod and cone photoreceptors (Hestrin and Korenbrot, 1990; Makino et al., 1991) and the small and rapid ionic channel gating currents in unicellular expression systems (e.g., Sheets et al., 1996). In bacteriorhodopsin the combination of ERP (photovoltage) and site-specific mutagenesis/expression techniques have been used to evaluate the contribution of select amino acid side chains to the vectorial charge motions that underlie the proton pumping mechanism (Moltke et al., 1992; Misra, 1998). Therefore, it was reasonable to explore the ERC as a time-resolved assay of electrically active conformational and chemical states during rhodopsin activation in an expression system where high plasma membrane rhodopsin levels could be achieved. A heterologous expression system was chosen to test whether ERCs could be recorded from expressed human rhodopsins in single cells. Reported values of activation currents from intact photoreceptors or rod outer segment disks are only a fraction of an equivalent electronic charge ($\approx$0.15e) moving across the entire membrane dielectric per rhodopsin molecule. Therefore, large numbers of rhodopsin molecules must be simultaneously activated to generate measurable ERCs. ERC signals are linearly proportional to the amount of rhodopsin activated until charge movements saturate at the highest flash intensities (Govardovskii, 1979; Hodgkin and O'Bryan, 1977; Drachev et al., 1981). There are four crucial factors to record ERCs from rhodopsin expressed in single cells in which opsin is expressed heterologously: the absolute quantity of opsin that is trafficked to the plasma membrane, the efficiency of regeneration with chromophore, the amount of light that can be delivered as a brief flash to activate the pigment, and a single cell electrophysiological recording apparatus to measure low amplitude signals above background noise at high temporal resolution. Preliminary calculations indicated that the opsin expression levels achievable in the HEK293S (human embryonic kidney) cells (Nathans et al., 1989) would be sufficient to record ERC R_2 signals given efficient pigment regeneration with 11-*cis*-retinal, a light intensity level on the order of 10^8 photons/μm^2, and a low noise whole-cell patch clamp data acquisition system with a bandwidth $>$1 kHz (Sullivan, 1996; Hamill et al., 1981). Moreover, HEK293 cells have low ion channel density, high membrane resistance and thus low current noise, which has supported their prior use in biophysical characterization of ionic currents of normal and mutant expressed ionic channels (e.g., Margolskee et al., 1993) and more recently, gating currents (e.g., Sheets et al., 1996), a challenge that was heretofore met only by bulk expression of channels in *Xenopus* oocytes. We anticipated that these properties of HEK293 cells would aid in recording ERC signals at reliable SNRs.

In this initial investigation we demonstrate that ERCs can be obtained from single or fused giant HEK293S cells expressing WT human rod opsin at densities comparable to that found in the plasma membrane of rod photoreceptors (Makino et al., 1991). ERC waveforms from the expression system are similar to those found in intact vertebrate rod photoreceptors. In fused giant cells ERCs are well resolved over whole-cell current noise. ERC charge motion results from the flash photolytic activation of expressed rhodopsin. The ERC is a kinetically complex signal suggestive of several contributing electrical states although the conformational/chemical transitions underlying these states remains to be determined. Most significantly, this approach resolves, in a single cell, conformationally dependent charge motions from about a picogram of rhodopsin with submillisecond time resolution. Our work not only brings time resolution to studies of rhodopsin in a physiologically intact heterologous unicellular expression system, but also extends sensitivity by 10^7-10^8-fold compared to other techniques currently used to study expressed visual pigments. The sensitivity of modern electrophysiological techniques permits this approach to structure-function studies of rhodopsin activation. The expression ERC assay established here is likely to become a useful tool in the characterization of rhodopsin conformational changes orthogonal to the chromophore plane, which are important in generating the R* conformation of not only rod but also cone pigments. This approach will likely be effective at characterizing mutant pigments that have perturbed R* formation. Our overall goals are to understand the molecular processes of charge redistribution during normal activation, to evaluate the forces contributing to these events and whether they cause protein conformational changes, and to investigate abnormal activation processes in laboratory-constructed mutants and naturally occurring mutant human rod pigments that cause retinal degenerations.

MATERIALS AND METHODS

Cell culture and fusion

Control HEK293S cells and an HEK293S cell line constitutively expressing WT human opsin (WT-HEK293) were grown at 37°C and 5% CO_2 in DMEM/F12 containing 10% (v/v) calf serum and antibiotics on poly-L-lysine-coated coverslips. Cells were chemically fused by transient exposure

to 50% (w/v) polyethylene glycol (1500 g/mol) in 75 mM HEPES (pH 8.0) (Boehringer-Mannheim, Indianapolis, IN) (Kersting et al., 1989). Fused giant cells formed within hours of polyethylene glycol exposure and were used for ERC recording between one and three days following fusion (Sheets et al., 1996).

Immunocytochemistry

WT-HEK293 and untransfected control HEK293S cells were grown on coated coverslips, and were fixed and permeabilized with ice-cold methanol. They were then exposed to a carboxyl-terminal rhodopsin monoclonal antibody (1D4) (Molday and MacKenzie, 1983) (10 μg/ml in 1× PBS, 10% goat serum) for 1 h at room temperature, washed with 1× PBS, reacted with a fluorescein isothiocyanate-labeled horse-anti-mouse monoclonal secondary antibody (10 μg/ml in 1× PBS, 10% horse serum), and photographed on a Nikon Microphot-FX fluorescent microscope (Nikon filter cube B-2E) with Kodak P1600 Ektachrome film.

Rhodopsin purification and absolute spectrophotometry

WT-HEK293 cells grown on 10-cm dishes were harvested in 1× PBS plus 5 mM EDTA and collected by gentle centrifugation. Rhodopsin was regenerated in 1× PBS with 15–20 μM 11-*cis*-retinal in darkness at 4°C for 2–3 h. Collected cells were solubilized in 1% DM (Anatrace, Maumee, OH) and the monodispersed rhodopsin was bound to excess (≥2-fold) immunoaffinity resin (1D4 covalently complexed to Sepharose-4B (Oprian, 1993). Unbound material was eluted in 1× PBS and rhodopsin was displaced from the resin with 35–50 μM of a synthetic peptide (14-mer) competing against the 1D4 epitope (Molday and MacKenzie, 1983). Absorption spectroscopy was used to quantify the amount of purified rhodopsin from populations of cells. A Beckman DU-640 UV-visible single beam spectrophotometer was used to acquire blank-subtracted spectra from 250–650 nm at 0.5 nm resolution. Absolute quantities of rhodopsin were determined from the extinction at peak absorption using the Beer-Lambert law and a molar extinction coefficient of 40,000 M^{-1} cm^{-1} for human rhodopsin (Wald and Brown, 1958; Knowles and Dartnall, 1977).

Flash photolysis

Rhodopsin regenerated in single cells was activated by a novel bright flash monochromatic microbeam apparatus described in detail elsewhere (Sullivan, 1998). In this study three-cavity bandpass filters were used to generate band-limited stimuli (center of transmission at 350, 430, 500, and 570 nm; 70 nm bandpass). The microbeam spot in the specimen plane was 228 μm in diameter (full-width, half-maximal). This is about three times the diameter of the largest giant cell which was studied and insured spatially uniform pigment photolysis in all cells. The instrument generates band-limited flashes between 10^8 and 10^9 photons/μm^2 across the near-UV through visible region in the specimen plane of the microscope. Flash duration was 14 μs at the full capacitor charge used in these experiments. This is sufficiently rapid such that in our experiments conducted at room temperature the Meta-I⇔Meta-II equilibrium should not be perturbed by photoregeneration from these states (Williams, 1964, 1965; Pugh, 1975). This is because the rate of formation of Meta-I from lumirhodopsin is ~1 ms at room temperature and the rate of formation of Meta-II from Meta-I is several milliseconds (Sengbusch and Stieve, 1971). In contrast, formation of lumirhodopsin is largely complete by 1 μs at room temperature (Lewis et al., 1989). Therefore, the lifetimes of early intermediates extending from bathorhodopsin to lumirhodopsin overlap with the flash duration and are susceptible to photoconversion to rhodopsin (493 nm) and isorhodopsin (480 nm). Because of electromagnetic and vibrational shielding and transmission of the flash on a fiber optic there are no flash-associated noise transients seen with patch clamp electronics.

Given the photosensitivity (P_t), which is the product of quantum efficiency (τ) and molecular absorption cross-section (α), the fraction (P_n) of rhodopsin molecules that absorb n photons per flash can be estimated from the Poisson equation $\{P_n = a^n \cdot \exp(-a)/n!\}$ where a is the product of the quantal efficiency (τ, taken as 0.67), the single flash photon density (i, in photons/Å^2), and the molecular cross-section (Å^2/molecule) ($a = \tau \cdot i \cdot \alpha_\lambda$), while n is the number of photons absorbed per molecule with each flash. The number that absorbs at least one photon is $1 - P_0 = 1 - \exp(-a)$. Calculating α_λ of human rhodopsin from the extinction coefficient (ϵ) at 493 nm (40,000 $M^{-1} \cdot cm^{-1}$) ($\alpha_\lambda = 3.82 \times 10^{-21} \cdot \epsilon_\lambda$), one arrives at a value of 1.23×10^{-8} μm^2 at 493 nm; α can be calculated for other wavelengths from the ratio of extinctions with respect to 493 nm. We take τ to be constant at different wavelengths (0.67) in the major rhodopsin absorption band. The maximum fraction of rhodopsin molecules absorbing at least one photon by a single flash using 70-nm bandwidth filters at 350, 430, 500, and 570 nm is calculated to be 0.16, 0.72, 0.96, and 0.27, respectively, at the flash intensities delivered in these experiments. Flash intensities were 8.02×10^7 photons/μm^2 (350 nm), 3.62×10^8 photons/μm^2 (430 nm), 4.07×10^8 photons/μm^2 (500 nm), and 3.38×10^8 photons/μm^2 (570 nm). This assumes no pigment orientational factors, no self-screening effects, and transparent cellular media. The maximum amount of rhodopsin that will go on to form Meta-II after a single flash is 50% (Williams, 1965) because of second photon resorptions during the early conformational transitions (e.g., bathorhodopsin, lumirhodopsin) which have high quantal efficiency to photochemically regenerate the ground state.

Cellular rhodopsin regeneration

Cells on coverslips were washed in regeneration buffer and placed in a light-tight container in the darkroom at room temperature (22–25°C). The protocol evolved during the course of these experiments. In initial experiments the regeneration solution contained (in mM): 140 NaCl, 5.4 KCl, 1.8 $CaCl_2$, 1.0 $MgCl_2$, 10 glucose, 10 HEPES-KOH, pH 7.2 (recording solution: E-0). An aliquot of 11-*cis*-retinal dissolved in ethanol was added to E-0 to a final concentration of 25 or 50 μM and cells were allowed to regenerate for at least 20–30 min (Wald and Brown, 1958). Final ethanol concentration was ~0.1%. After ERC signals were extinguished by several flashes, rhodopsin was regenerated by local perfusion of 25–50 μM 11-*cis*-retinal in bath solution using a microperfusion pipette under electronic microvalve control. However, addition of concentrated stocks of 11-*cis*-retinal in ethanol to aqueous solutions was neither the most efficacious nor rapid method of regenerating rhodopsin from opsin (Szuts and Harosi, 1991; McDowell, 1993). In later experiments, which includes all giant cell studies reported here, a more efficient regeneration solution was used (in mM): 140 NaCl, 5.4 KCl, 1.8 $CaCl_2$, 1.0 $MgCl_2$, 10 glucose, 10 HEPES-NaOH, pH 7.2, and 2% (w/v) fatty acid-free bovine serum albumin (FAF-BSA) (≈290 μM) (Sigma, St. Louis, MO). 11-*cis*-Retinal in ethanol was added to this solution to a final concentration of 50 μM in preliminary experiments and 25 μM in the final protocol with 0.025% (v/v) α-D-tocopherol (vitamin E) added as an antioxidant (Szuts and Harosi, 1991). Vitamin E is an antioxidant found in millimolar concentration in photoreceptors (Dilley and McConnell, 1970). Regeneration with FAF-BSA was conducted for at least 30 min in the dark at room temperature when coverslip fragments were washed in bath recording buffer and transferred to the recording chamber (both without 11-*cis*-retinal). Once in the recording chamber cells were not again exposed to exogenous 11-*cis*-retinal unless otherwise stated. The FAF-BSA molecule binds retinal and can exchange chromophore rapidly and stoichiometrically to regenerate rhodopsin from opsin (McDowell, 1993). An indication of retinal solubilization comes from the lack of visible optical scattering (optically clear yellow solution) upon addition of concentrated ethanolic stocks of chromophores into albumin-containing solutions. When ethanolic stocks of retinal were added directly into bathing solutions that did not contain FAF-BSA in the initial experiments, significant light scattering occurred (cloudy yellow-white solution), which indicated poor solubilization and extensive partitioning of the hydrophobic chromophore out of aqueous solution.

Whole-cell ERC recording

Cells on coverslips were imaged using infrared light (high-pass cutoff 830 nm) at 80–160× by a Nikon Diaphot inverted microscope equipped with Nomarski differential interference contrast (Nikon, Tokyo, Japan), a CCD camera, and a TV monitor covered with a long-pass filter. The microscope was housed in a light-tight Faraday cage in a dark room. Pipettes were fashioned from borosilicate glass (Kimax 51) using two stage pulls and coated with Black Sylgard (#173, Dow Corning, Midland, MI). Electrodes were not fire-polished, had bubble numbers of 5.4 in methanol (Corey and Stevens, 1983) and resistances ~8 MΩ. In initial ERC experiments on single cells the electrode was filled with (in mM): 120 KF, 10 KCl, 1.0 $CaCl_2$, 2.0 $MgCl_2$, 11.0 EGTA-KOH, 10 HEPES-KOH, pH 7.2) (solution I-0) and the bath contained the initial regeneration buffer (above) without 11-*cis*-retinal (solution E-0). In later experiments involving albumin-facilitated regeneration on single or giant cells, pipettes were filled with one of two intracellular solutions (with or without 10 HEPES-CsOH) (in mM): 70 tetramethylammonium hydroxide (TMA-OH), 70 2-[*N*-morpholino]ethanesulfonic acid (MES-H), 70 TMA-fluoride, 10 EGTA-CsOH, 10 HEPES-CsOH, pH 6.5) (solution I-1); the presence of 10 HEPES-CsOH caused no qualitative changes in the ERC signal. The pH of the internal solution (pH = 6.5) was chosen to bias the Meta-I⇔Meta-II equilibrium strongly in favor of Meta-II (>90%) at room temperature (Parkes and Liebman, 1984). The bath solution contained (in mM): 140 TMA-OH, 140 MES-H, 2.0 $CaCl_2$, 2.0 $MgCl_2$, 5.0 HEPES-NaOH, pH 7.0 (solution E-1). In these solutions (E-1, I-1) the TMA^+ and MES^- ions represent the bulk charge carriers both inside and outside the cell and are largely impermeant through fused HEK293 cell plasma membranes where they were previously used in the same context for gating current recordings (Sheets et al., 1996). In these solutions fused giant HEK293 cells remained well-attached to the treated glass substrate with apparent spherical geometry.

Fused giant cells readily formed gigaohm seals, patch/seal capacitance was compensated, and whole-cell recording was easy to achieve with further suction. ERC signals were regularly generated when fused cells were used between the first and third days after fusion. The patch clamp instrument was an Axopatch 1C with a CV-4 resistive feedback headstage (Axon Ind, Foster City, CA). In most of the ERC experiments the membrane potential was clamped constantly at 0 mV (exceptions are stated in the figure legends). Since the ERC is a capacitative current ($I_{erc} = C_{mem} \cdot dV_{ERP}/dt$) the whole-cell capacitance (C_{mem}) and series resistance (R_{ser}) were not electronically compensated in these experiments (see below). Whole-cell capacity current was acquired with a +20 mV/4 ms test pulse from a holding potential of −80 mV and C_{mem} was computed by first subtracting ohmic current and then integrating the capacitative current waveform to obtain charge (Q; $Q = C_{mem} \cdot V$). The surface area was estimated from the measured C_{mem} (1 $\mu F/cm^2$) and was compared to that obtained from the cell diameter (spherical surface area = πd^2). The electrically derived areas were typically larger and consistent with spare membrane (e.g., microvilli) not appreciated from caliper measures of diameter. Cell volume was computed from the spherical cell diameter ($V = (1/6)\pi d^3$). Ramp voltage clamps were used to test membrane resistance and the level of leakage current. Cells with large leakage currents were discarded. The ramps were initiated from a holding potential of −80 mV and conducted from −100 mV to +100 mV over 1 s. Inward and outward rectifying conductances are present in HEK293 cells but were suppressed by the permeant ion replacement solutions used in the pipette and bath in the later experiments. Whole-cell ERC currents were recorded at 5 kHz bandwidth using an 8-pole Bessel filter and data were digitized at 200 μs/point. This undersamples the R_1 kinetics but allows high-fidelity recording of the entire R_2 signal, which has a slow relaxation tail (<100 ms). Flashes were controlled and data acquired using pCLAMP 5.51 (CLAMPEX; Axon Ind., Foster City, CA) and a Scientific Solutions data interface as previously described (Sullivan, 1998). ERC data were analyzed using Origin 4.1 (Microcal Software, Northampton, MA).

The mean ERC action spectra were fit with a symmetrical Voigt function (below) which is the closest approximation to a Dartnall isotherm for the number of points obtained that maintains all parameters floating. The Voigt function might also be viewed as appropriate to fit both the Lorentzian lifetime of the absorbing state and the Gaussian broadening that would result from use of the wide-band interference filters used to deliver the flash stimulus (see Fig. 9). In this function x is the wavelength, x_c is the center (peak) wavelength, w_G and w_L are the Gaussian and Lorentzian peak widths, A is the amplitude scaling function, Q_o is the y offset, and t is the sensitivity parameter.

$$Q = Q_o + A \cdot 2 \cdot \ln 2/\pi^{3/2} \cdot w_L/w_G \cdot \int_{-\infty}^{\infty} e^{-t} dt$$

$$\times\{(\sqrt{\ln 2} \cdot w_L/w_G)^2 + (\sqrt{4 \cdot \ln 2} \cdot (x - x_c)/w_G - t)^2\}^{-1}$$

R_2 kinetic relaxations were fit with a sum of exponentials (Fig. 10) (double exponential shown) where A1 and A2 are the weighting parameters to the two respective time constants (τ_a, τ_b), and t_o is the time point in the ERC record in which fitting was commenced (after the R_2 peak).

$$ERC(t) = A1 \cdot e^{-(t-t_0)/\tau a} + A2 \cdot e^{-(t-t_0)/\tau b}$$

Histograms were fit with a single Gaussian model (Fig. 11 *D*) (equation not shown). In all cases nonlinear curve fitting employed a Marquardt-Levinberg nonlinear least-squares fitting algorithm (Origin 4.1). Simple linear fits used the regression package in Origin 4.1.

The whole-cell charging time constant under voltage clamp recording is approximated by the product of C_{mem} and R_{ser} (Marty and Neher, 1983). Simultaneous amplifier compensation (electronic) of R_{ser} and C_{mem} are usually coordinated to improve the speed of voltage clamp recording and the poles of these compensations are typically not independent. Since the ERC is a capacitative current, compensation of C_{mem} (and R_{ser}) might affect the amplitude or kinetics of net charge motions. Compensation appeared unnecessary and was not used. Membrane potential was not simultaneously perturbed concurrent with stimulus flashes. In preliminary experiments combined C_{mem} and R_{ser} compensation had no apparent effect on the kinetics of the R_2 relaxation of the WT ERC. ERCs were acquired without R_{ser} or C_{mem} compensation in previous ERC studies on photoreceptors (Makino et al., 1991). Lack of R_{ser} compensation is expected to have a minimal effect on clamp of constant holding potential since the largest ERC currents recorded would generate only small voltage errors across R_{ser} (≈1 mV). The charging time constants to a voltage step were estimated to range from ~250 μs to 2.5 ms using the measured range of C_{mem} (12.5–125 pF) and estimating R_{ser} to be ~20 MΩ.

RESULTS

WT human opsin cell line constitutively expresses high levels to the plasma membrane

WT human rhodopsin was immunoaffinity purified from WT-HEK293 cells solubilized in 1% DM after regeneration with excess 11-*cis*-retinal. Dark-adapted rhodopsin from a sucrose density gradient preparation (band II) of bovine retina was also solubilized in 1% DM and purified over 1D4-Sepharose. Samples were examined by spectrophotometry and the absorbance spectra plotted (Fig. 1). The major α- (≈500 nm), β- (350 nm), and γ-bands (280 nm) are as previously reported for vertebrate A_1 pigments (Wald and Brown, 1958). The 11-*cis*-retinal β-band and the protein γ-band show similar peak wavelengths in the native bovine and expressed human rod rhodopsin pigments, while the human α-band is blue-shifted with respect to the bovine pigment. The normalized spectra show this shift (*inset*) with the bovine peak at 498 nm and expressed human rod rhodopsin peak at 493 nm. This is consistent with the spectral

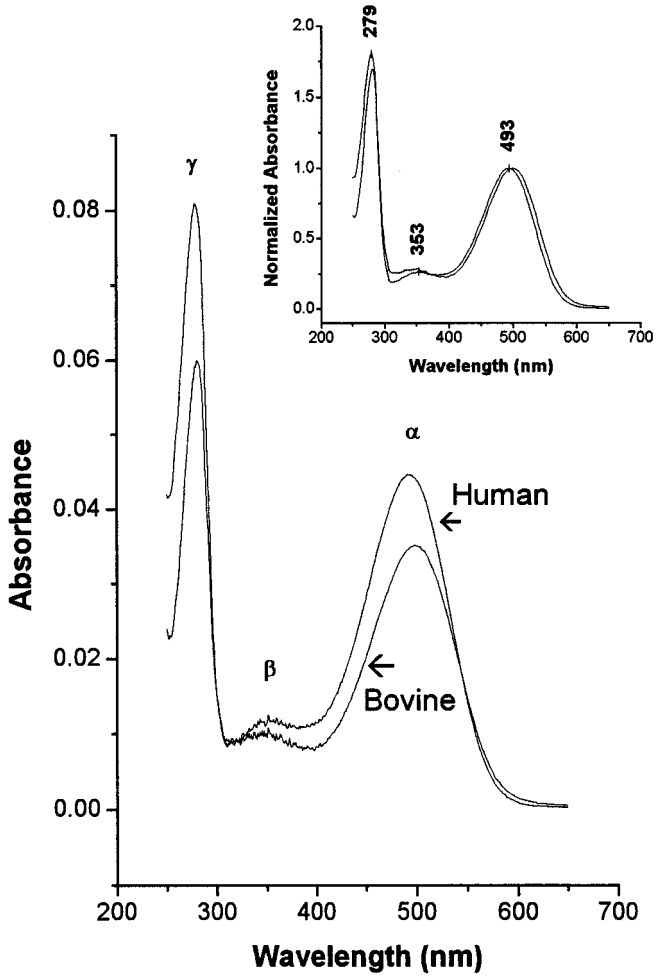

FIGURE 1 Spectrophotometry of rhodopsin in WT12 cells. Normal human rhodopsin was purified over 1D4-Sepharose from WT-HEK293 cells following regeneration with 16 μM 11-*cis*-retinal for 3 h at 4°C and extraction in 1% DM in 1× PBS. Bovine rhodopsin was similarly extracted from a sucrose step preparation (band II) of dark-adapted bovine retina. In both cases pigment was eluted from the resin with 35 μM of a 14-mer peptide complementary to the carboxyl-terminus of human and bovine rhodopsin that contains the 1D4 recognition epitope. Relevant absorption bands and the peak wavelengths of the pigments are illustrated. The bovine spectrum was scaled to match the absorbance at peak extinction of the human pigment such that the peak wavelengths could be more readily compared (*inset*).

maximum (493 nm) of native human rhodopsin extracted from cadaver eyes with 2% digitonin in PBS (Wald and Brown, 1958). The spectral ratios of OD_{540}/OD_{493} and OD_{390}/OD_{493} of native human rod rhodopsin were 0.436 and 0.24, respectively, whereas expressed human rhodopsin in 1% DM in PBS had comparable ratios of 0.469 and 0.247. The ground state of expressed human rhodopsin acid traps to a peak around 440 nm and upon exposure to light $\geq$540 nm it quantitatively transforms to a spectral state absorbing ~380 nm, consistent with Meta-II (data not shown). Thus, human rhodopsin expressed in WT-HEK293 cells has essentially identical spectral properties compared to native human rhodopsin.

Spectrophotometry was used to quantitate total regenerable rhodopsin in the WT-HEK293S cell line used in these experiments (Fig. 1). Using Beer's law, the extinction coefficient of WT rhodopsin, the absorbance at maximum extinction (493 nm) and the sample volume, one finds that 17.8 μg of regenerable opsin was made in 3×10^7 cells leading to an average value of 8.9×10^6 rhodopsins/cell in this preparation. Other preparations gave similar values (mean $\pm$ SD: $6.3 \pm 2.6 \times 10^6$ rhodopsins/cell, $n = 3$). Expressed, regenerated, and purified human rhodopsin has an A_{280}/A_{493} between 1.8 and 2.0, indicating a high degree of purification near the theoretical limit of the spectroscopic ratio (Hong and Hubbell, 1973).

Immunocytochemistry was used to localize opsin protein expressed in WT-HEK293 cells. Immunofluorescence demonstrated essentially all reactivity above background in the plasma membrane. Most of the opsin expressed in this cell line trafficks to the plasma membrane and each cell in the population expresses opsin at uniform levels (Fig. 2 *A*). Untransfected HEK293S cells show only faint background fluorescence (Fig. 2 *B*), which reflects cellular flavinoids (Zylka and Schnapp, 1996). A constitutively expressing opsin cell line makes ERC recording easier, because each cell sampled by flash photolysis contains opsin at uniform plasma membrane levels. This is in contrast to most cells in a transiently transfected population, which do not express opsin. Furthermore, those that do (e.g., 5–20% with calcium phosphate or electroporation protocols in our hands) have nonuniform expression levels because of variation in plasmid load (data not shown). Polyethylene glycol fusion of constitutively expressing WT human opsin cells also lead to giant cells with a uniform distribution of WT opsin in the plasma membrane reflecting that of the contributions of individual cells (Fig. 2, *C* and *D*). Fusion of constitutively expressing cells is expected to yield absolute levels of plasma membrane visual pigment in proportion to the number of fused cells.

Early receptor currents recorded from human rhodopsin in single WT-HEK293 cells

If all of the $\approx 9 \times 10^6$ rhodopsins/cell are in the WT-HEK293 plasma membrane, the mean single-cell surface area (assuming spherical geometry) of 785 μm^2 (mean single cell diameter $\pm$ SE: 15.8 ± 2.1 μm, $n = 20$) leads to a calculated opsin membrane density of 1.1×10^4 rhodopsins/μm^2. This approximates that found in the rod outer segment disk membranes (2.7×10^4 rhodopsins/μm^2) (Liebman et al., 1974). Surface human opsin density in HEK293S plasma membranes implies a diffusional environment similar to the photoreceptor, although the lipid composition is likely to be different (Weitz and Nathans, 1993). The absolute numbers of plasma membrane rhodopsin molecules in single WT-HEK293 cells approximate the amount found in giant amphibian rod photoreceptors that supported strong ERC signals ($1.2–1.9 \times 10^7$ rhodopsins/

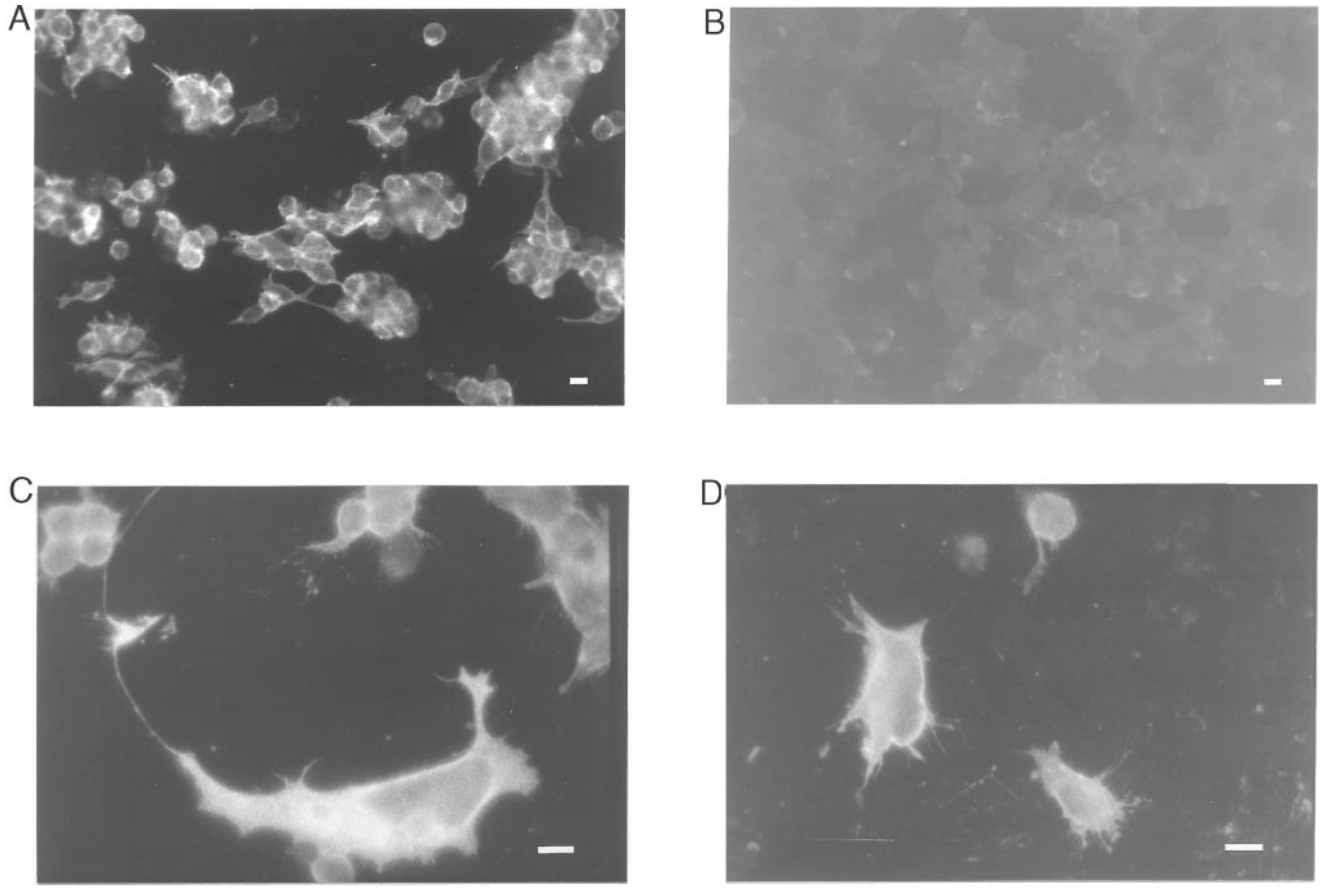

FIGURE 2 Immunocytochemistry of rhodopsin in HEK293 Cells. WT-HEK293 cells and HEK293S cells were grown on poly-L-lysine-coated coverslips. Polyethylene glycol fusion of WT-HEK293 cells was conducted on coverslips. (*A*) WT-HEK293 cells. (*B*) HEK293S control cells. (*C*) Single fused giant WT-HEK293 cell with attached single unfused cell. (*D*) Two fused giant cells. The photographs of the fused cells were obtained at twice the magnification of the unfused cells. Scale marker is 20 μm in all.

cell) (Makino et al., 1991; see Fig. 4). This suggested that ERC signal strength in WT-HEK293 cells would be comparable within an order of magnitude. Assuming a unitary charge motion of 0.15e/R* during R_2 (Govardovskii, 1979; Hochstrate et al., 1982; Makino et al., 1991), a maximum of only 50% of available plasma membrane rhodopsin charge moving with each saturating flash (Williams, 1965; Pugh 1975), no instrumentation delays, and an R_2 charge motion occurring in a single step coordinated with the rate of Meta-II formation ($\approx$2 ms at room temperature), a maximum ERC amplitude of $\sim$50 pA and a total bleach ERC charge movement of $\sim$0.2 pC was estimated. Signals of this amplitude are recordable with a conventional whole-cell gigaohm-seal voltage clamp with millisecond-order resolution. ERC recordings at reasonable SNR were anticipated with multiple ERCs expected from each cell before complete bleaching of the plasma membrane rhodopsin.

Fig. 3 *A* shows ERCs resulting from sequential flashes in a WT-HEK293 cell that was regenerated with 50 μM 11-*cis*-retinal (without FAF-BSA) and subjected to whole-cell recording without permeant ion replacement (solutions E-0/I-0). Upon each stimulus (500 nm, 4.08×10^8 photons/μm^2) transient outward currents were found similar in shape and time course to ERC R_2 currents of amphibian photoreceptors (Hestrin and Korenbrot, 1990; Makino et al., 1991). An R_1 phase was not observed probably because of relatively smaller R_1 charge motions and whole-cell background current noise (20–40 pA peak-peak in this cell). On the first flash the ERC R_2 wave peaked at $\sim$99 pA (signal plus noise). The first three flashes promoted progressive extinction of the ERC signal without apparent change in the waveform, and no discernible signal was present above background noise after the fourth flash. After the sixth flash the region around the cell was perfused for 1.5 min with a micropipette containing 11-*cis*-retinal (50 μM) in normal bath solution (E-0). About 4 min after the start of retinal perfusion, flashes elicited small extinguishable ERC currents indicating partial reconstitution of the original signal and with similar kinetics as that found on the first flash (Fig. 3 *B*). After subtraction of baseline current the amount of R_2 charge moved with each 500-nm flash (Q_i) was determined by integrating the ERC waveform. Mean R_2 charge versus flash number is plotted for several single cells regenerated with 11-*cis*-retinal upon addition of raw ethanolic stocks or BSA-complexed solutions (Fig. 3 *C*). ERC extinction data were fit with a single-exponential decay curve, consistent

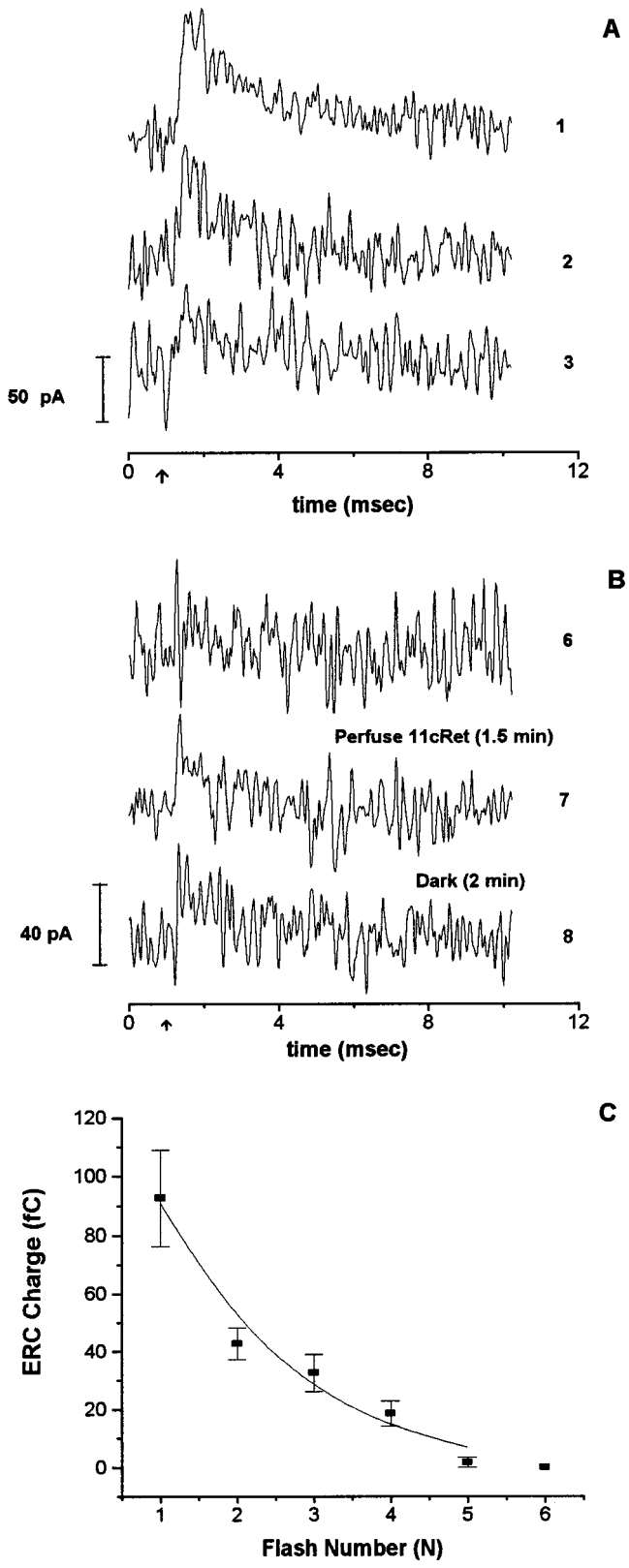

FIGURE 3 ERC Recordings from single cells. (*A*) An unfused WT-HEK293 cell was subjected to serial flash photolysis at 500 nm. Arrow indicates 500-nm flash. E-0 was the solution in the bath and I-0 was the solution in the pipette and membrane potential was clamped at −30 mV. (*B*) Following extinction of the ERC signal, 50 μM 11-*cis*-retinal in E-0 buffer was perfused with a micropipette placed near the cell for 1.5 min. ERCs recovered with perfusion of 11-*cis*-retinal. (*C*) Mean ERC charge motion (Q_i) (±SE) versus flash number (*N*) were determined for three cells. In two cells the holding potential was −30 mV and in one it was 0 mV. The curve fit to the data is a single exponential of the form: $Q_N = Q_\infty \cdot \exp^{-P \cdot N}$, where Q_∞ is the extrapolated charge present before any flashes are given and P is the bleaching sensitivity factor. The fitted value of Q_∞ was 166.2 fC, whereas the experimentally determined mean (±SE) of Q_∞ for three cells was 188.2 ± 31.4 fC (215.7, 223.4, and 125.5 fC). The fitted bleaching sensitivity factor was 1.73, which corresponds to a photosensitivity ($\alpha \cdot \tau$) of $\sim 1.54 \times 10^{-9}$ μm^2. The correlation coefficient (*R*) of the fit was 0.986 ($p < 0.05$).

with a bleaching experiment where each rhodopsin molecule behaved independently. The individual integrated Q_i responses were summed to give the total ERC R_2 charge mobilized in each cell during complete extinction (Q_∞) (mean ± SE: 188.2 ± 31.4 fC, $n = 3$ cells). With 0.15e/R* as the unitary charge motion, a mean total of 7.8×10^6 rhodopsins/cell were activated and bleached by the flashes in the extinction experiments. This agrees with previous spectrophotometric estimates of the amount of rhodopsin/cell. Hence, the ERC can be used as a "measure" of the quantity of ground state plasma membrane rhodopsin (Cone and Pak, 1971; Lisman and Bering, 1977). Each activated rhodopsin molecule makes a linear contribution to the total charge flow and current and essentially all of the WT rhodopsin purified from this cell line must originate from the plasma membrane (Nathans et al., 1989) where it can be measured electrophysiologically with the ERC. The mean Q_∞ value and the mean number of rhodopsins/cell (above) were used to calculate the unitary charge motion (0.186e/rhodopsin), which approximates the values found in photoreceptors (≈0.15e/rhodopsin). Although ERC signals acquired from single WT-HEK293 cells were encouraging and consistent with anticipated signal characteristics, the total charge motion was low, regeneration was only partial, and repetitive addition of membrane-toxic, ethanol-containing solutions of 11-*cis*-retinal were necessary.

Early receptor currents recorded from fused giant cells

Fused giant cells were made from single WT-HEK293 cells with the expectation that increased numbers of plasma membrane rhodopsin molecules would allow larger ERC signals at improved SNR. This was based upon the fact that ERC charge motion is linearly proportional to the numbers of rhodopsins activated until saturation (Cone and Pak, 1971). As shown above, chemically fused giant cells share a uniform distribution of immunocytochemically reactive plasma membrane opsin with single cells (Fig. 2, *C* and *D*). Flash photolysis of giant cells proved an increased total ERC charge and improved SNR. R_2 signals are sufficiently large to support quantitative study of the biophysics of charge motion. The R_1 phase of the ERC was readily recorded above noise and a broader dynamic range of

charge motion in the R_2 relaxation were resolved in giant cells. A surprising advantage of the giant cell system was that the primary pigment regeneration, accomplished with 11-*cis*-retinal complexed to FAF-BSA, removed the need for repetitive exposure of cells to exogenous 11-*cis*-retinal after flash-photolytic extinction of the ERC signal. FAF-BSA promotes loading of chromophore into cells during the initial regeneration and allows recovery of ERC signal (i.e., rhodopsin regeneration) after plasma membrane rhodopsin is bleached with no exogenously added 11-*cis*-retinal. In all giant cell experiments primary pigment regeneration occurred with 11-*cis*-retinal complexed to FAF-BSA in the dark for over 30 min. ERCs were elicited and ultimately extinguished by several flashes in the primary flash series. After signal extinction, which occurs secondary to progressive rhodopsin bleaching, giant cells were kept under whole-cell recording in the dark in the absence of experimentally added 11-*cis*-retinal. When secondary flash series were presented after 10 min in darkness, strong ERC signals were elicited. The spontaneous recovery of the ERC in the dark suggested that bleached opsin was regenerating with a source of chromophore. This pigment regeneration process appeared similar to recovery of rod photoreceptors from bleaching adaptation during the visual cycle in the intact retina. It is known that FAF-BSA facilitates the rapid delivery of chromophore to bleached photoreceptor rod outer segments to fully reconstitute rhodopsin (McDowell, 1993). This facilitation occurs because the FAF-BSA efficiently solubilizes retinal chromophores in aqueous solutions and allows abundant partitioning of the hydrophobic chromophore across the plasma membranes of rod outer segments into disk membranes that contain the largest fraction of regenerable opsin. It would appear that a similar bulk physical partitioning process also occurs in WT-HEK293 cells, and given that these cells are epithelial in origin may allow them to take up additional BSA-bound chromophore by pinocytosis. Recent experiments have determined that the source of the chromophore for spontaneous regeneration of the pigment in darkness is the internal membranes of the cell under recording (Shukla, Brueggemann, and Sullivan, work in progress). FAF-BSA regeneration loads sufficient chromophore into the abundant internal membranes of giant cells such that spontaneous regeneration of plasma membrane rhodopsin can occur rapidly.

Fig. 4 compares ERC signals from single and fused giant cells regenerated with 11-*cis*-retinal by the FAF-BSA method for over 30 min. Fig. 4 *A* shows a giant cell ERC obtained on the first flash (500 nm). The kinetically unresolved negative R_1 wave and the slower, larger, and positive R_2 wave are clearly evident. The transition from R_1 to R_2 is distinct, given a clear peak to the R_2 signal. By integrating the currents of the respective waves the total charge motion attributable to the R_1 and R_2 signals was obtained. The ERC signals generated after FAF-BSA 11-*cis*-retinal regeneration in giant cells are comparable to those seen in intact photoreceptors (Hestrin and Korenbrot, 1990; Makino et al., 1991) given that both components of the waveform are present in identical polarity, the relative quantity of charge moving in the R_1 and R_2 phases is similar, and the kinetics of the signal are also similar. In comparison, Fig. 4 *B* shows an initial ERC from an unfused single cell. The signal is smaller than that of the giant cell and no clear R_1 phase is identifiable. Charge motion signals in each cell were extinguished with successive flashes and then a 10-min period of darkness followed without further chromophore addition. Fig. 4, *C* and *D* show the ERCs in response to the first flash after the period of darkness in the same giant and single cells, respectively. R_2 waves were strong but R_1 signals were not present in either single or giant cells. The relative extent of spontaneous R_2 signal recovery in giant cells is large compared to single cells. Moreover, following spontaneous recovery the SNR was low in single cells relative to giant cells. A surprising finding was that the R_2 charge moved is greater in the giant cell after the R_1 phase is lost on the first extinction. The mechanism of R_1 loss is not clear, but the presence of an R_1 charge flow may inhibit outward R_2 charge flow. We are actively investigating which factors control the presence of the R_1 signal in the ERC (Brueggemann and Sullivan, work in progress). Since R_1 has a distinct peak on a millisecond time scale, mechanistic interrelationships with the millisecond-order R_2 signal are possible. Loss of R_1 allows R_2 to be studied in isolation in secondary flash series.

The percentage of fused giant cells showing quantifiable ERC signals similar to those in photoreceptors was 71% (56 of 79 cells) in our initial experience with this new approach. Most of the remaining cells lacked ERCs for unclear reasons and features of the cells (e.g., culture age, fusion date, membrane leakiness) are being catalogued in attempt to identify the relevant parameters. It is likely that these cells also contain uniform quantities of plasma membrane rhodopsin. Some of the remaining cells generated brief outward "spike" currents of ~1 ms in duration in response to flashes. We saw these signals when cells were stressed during growth (e.g., decreased media pH). Before the TMA/MES ion replacement solutions and the FAF-BSA/vitamin E regeneration techniques were used, flash-activated currents were recorded with broader R_1 signals (or inverted R_2 signals) followed later by a small outward-directed R_2 hump. Both of these signal types bleached following successive stimuli within the rhodopsin major absorption band and presumably represented a unique state of the rhodopsin pigment (data not shown). Recent experiments find almost all WT-HEK293 giant cells have measurable ERC signals when series resistance is low, and cells have nonleaky membranes with little current noise (Brueggemann and Sullivan, work in progress), suggesting that the initial recording failure rate of 29% was probably due to signal shunting.

ERC signals scale with the size of the fused cell

Fig. 5 *A* shows representative pictures of fused giant cells along with unfused cells (scale marker is 20 μm). In some

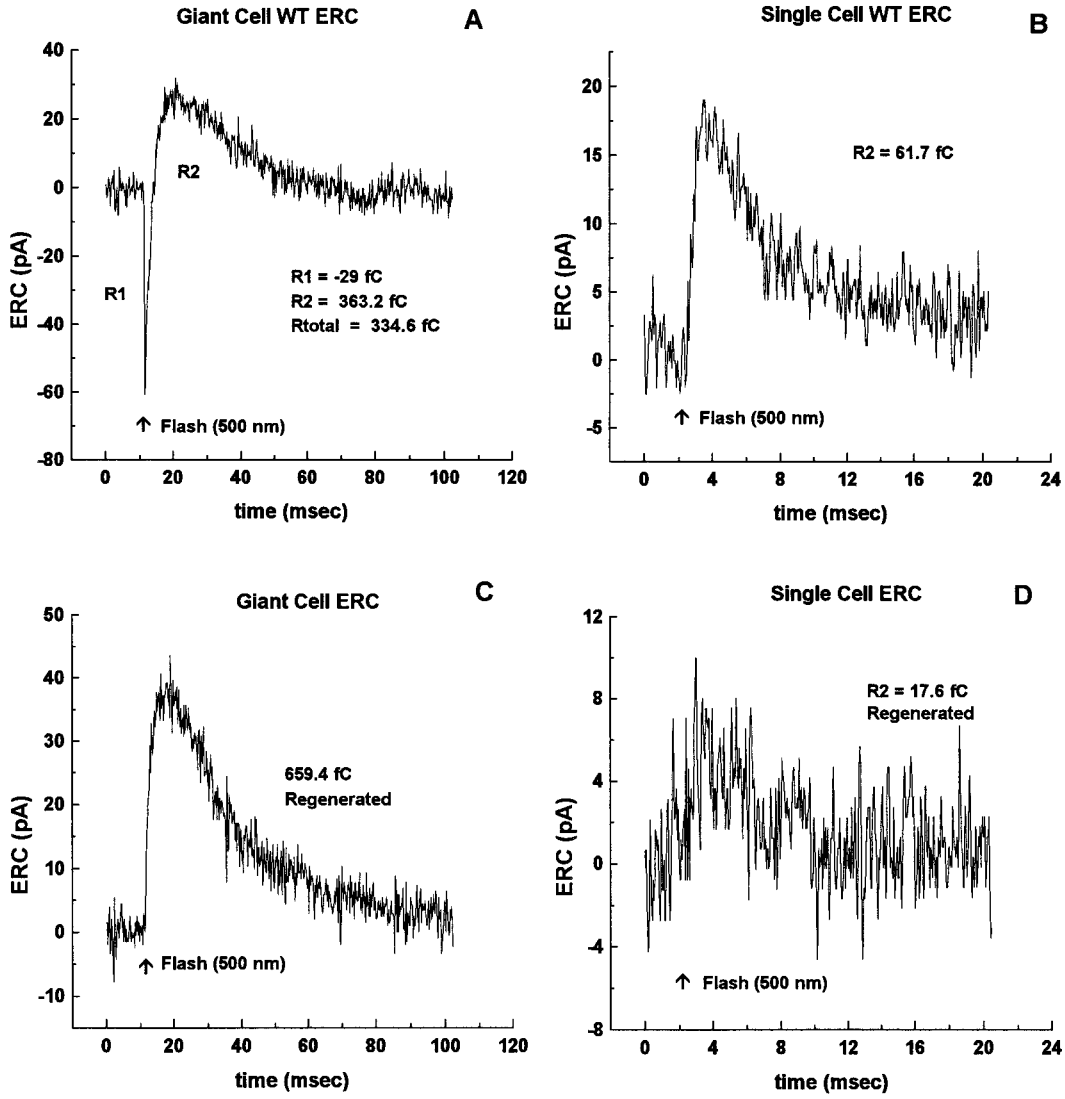

FIGURE 4 Comparison of ERCs from single and fused giant cells. Cells were regenerated using FAF-BSA, 25 μM 11-*cis*-retinal, and 0.025% (v/v) α-D-tocopherol in E-0 for over 30 min at room temperature. Cells were subjected to whole-cell recording using E-1 in the bath and I-1 in the pipette. Flashes were 500 nm and were given 2 ms or 10 ms into the start of each record for the single and giant cells, respectively. (*A*) ERC from a fused giant cell (68 pF) (first flash after primary regeneration). (*B*) ERC from a single cell (11 pF) (first flash after primary regeneration). (*C*) ERC from the fused giant cell, after previous extinction of signal and 10 min of dark adaptation without added 11-*cis*-retinal (first flash). (*D*) ERC from the single cell, after previous extinction of signal and 10 min of dark adaptation without added 11-*cis*-retinal (first flash). Note the difference in time and amplitude scales for the two cells.

fused cells a number of unfused nuclei can be seen. Total integrated ERC R_2 charge motions (Q_∞) were found to be linearly dependent upon both cell surface area (C_{mem}) and volume (Fig. 5, *B* and *C*). These data include recordings from both single and fused cells. A regression line reliably represented the data of Fig. 5 *B* and passed through the origin (0 fC, 0 pF) without constraint fitting both single and fused cell responses. This indicated that as the surface area of the cell increased, indicating larger numbers of opsin-expressing cells participating in the fusion event, total ERC charge increased linearly. The data also imply that the ERC signal resulted from flash photolysis of oriented pigment in the plasma membrane of WT-HEK293 cells and that opsin density remained uniform during the fusion of single cells to form giants. These data are consistent with previous work, which demonstrated that the ERP is linearly proportional to the amount of oriented rhodopsin in the plasma membrane (Cone and Pak, 1971; Lisman and Behring, 1977). Each fusing cell contributes a "quantum" of opsin to the plasma membrane of the fused giant cell. From the slope of the line (0.01149 ± 0.0025 SD pC/pF) a mean density of $\sim 4800 \pm 1053$ rhodopsin molecules/μm^2 was calculated for both fused and single cell membranes assuming 0.15e/R* as the unitary charge motion of R_2 (Makino et al., 1991). In contrast, if the membrane density is known, then the unitary charge motion can be calculated from the slope of the regression line. The density calculated approximates the rod outer segment disk membrane density ($3800/\mu m^2$) in rat

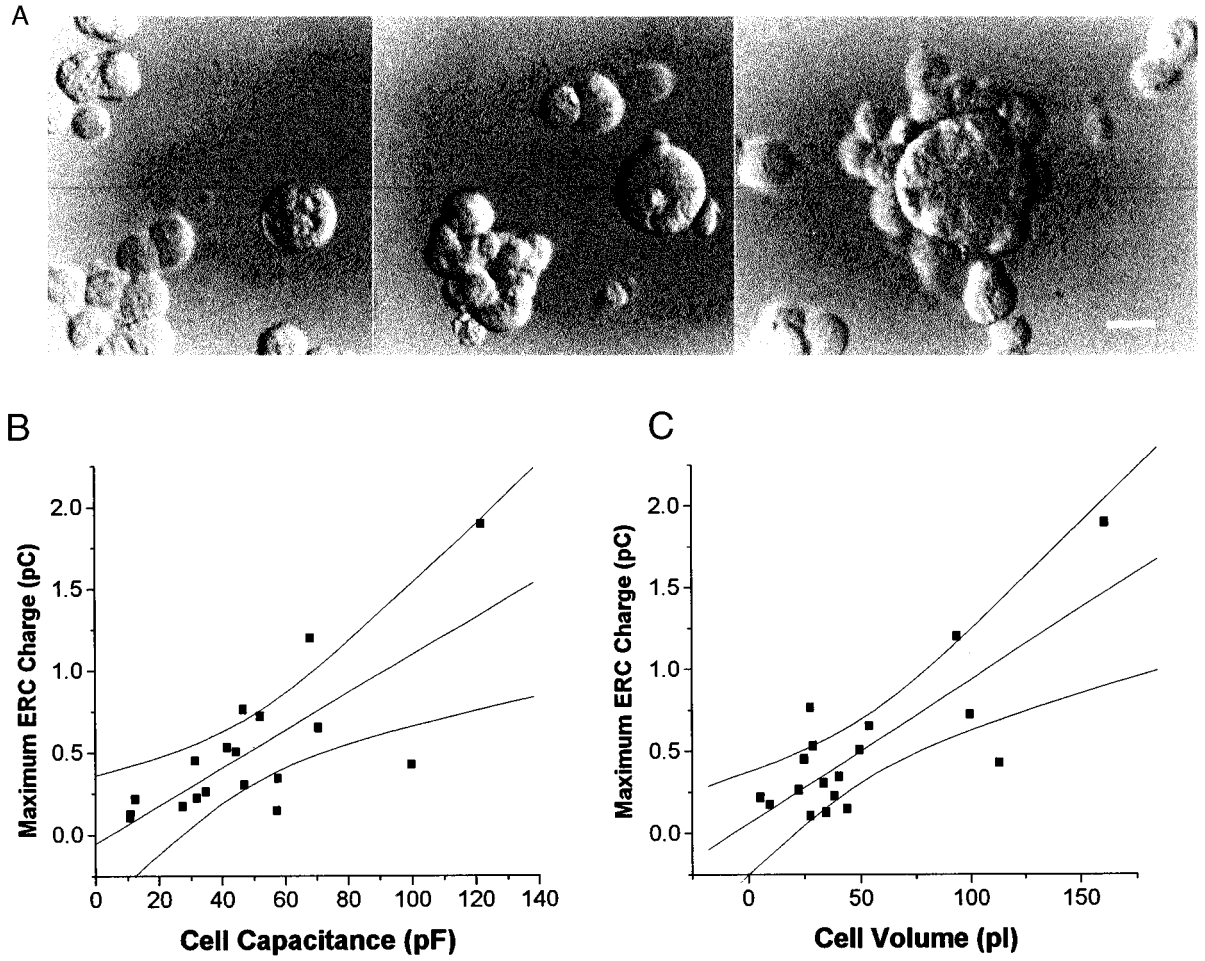

FIGURE 5 ERC Signals scale to the size of the cell. (*A*) Hoffmann contrast image of three examples of fused giant cells of different sizes surrounded by unfused single cells. (*B*) Total ERC charge (Q_∞) at 500 nm for many ($n = 18$) fused giant and single cells versus C_{mem} as a measure of cell surface area. In 15 cells the holding potential was 0 mV and in three cells it was +30 mV. Those held at +30 mV had charge motions that were also inside the confidence bands for both (*B*) and (*C*). The linear regression had the following characteristics: slope (0.01149 ± 0.0025 SD pC/pF), *y*-intercept (−0.051), correlation coeff. (0.75, $p = 3.4E\text{-}4$). (*C*) Total ERC charge (Q_∞) versus cell volume. The linear regression had the following characteristics: Slope (0.00875 ± 0.0017 SD pC/pl), *y*-intercept (0.0606), correlation coeff. (0.79, $p = 0.0001$). The 99% confidence bands on the regression line are also plotted in (*B*) and (*C*).

photoreceptors (Miyaguchi et al., 1992) and is ~6-fold less than the density in the rod outer segment disk or plasma membranes (27,000/μm^2) in amphibian photoreceptors (see Makino et al., 1991). Assuming the unitary charge (0.15e/R*) the absolute quantity of plasma membrane rhodopsin in fused giant cells ranged from ~0.4 to 5.25 pg or between 6×10^6 and 8×10^7 molecules. The total amount of rhodopsin in a mammalian rod photoreceptor is ~7 pg with most of this localized in internalized disks. Although the plasma membrane rhodopsin density in the HEK293 expression system approximates that found in mammalian or amphibian rod photoreceptors, in most fused giant cells the absolute amount of plasma membrane rhodopsin must be greater than in amphibian rods given the measured WT-HEK293 giant cell Q_∞ values versus those found in photoreceptors (mean $Q_\infty = 290 \pm 80$ fC) (Makino et al., 1991). This explains how ERC recordings from giant cells can be larger than those previously measured in tiger salamander rods, although the light intensities we used were usually higher (Makino et al., 1991).

ERC Q_∞ is also linearly proportional to cell volume. Fig. 5 *C* shows the total R_2 charge motion in relation to cellular volume estimated from the measured diameters of both single and fused giant cells. A regression line was fit to the data indicating that the ERC scales linearly with cell volume. Polyethylene glycol fusion is known to be an isovolumic process that promotes loss of membrane surface to maintain the surface/volume ratio (3/r) (Kersting et al., 1989). Therefore, by dividing the giant cell volume by that of the average single cell one can estimate how many cells fused to generate giant cells (4–75 cells, $n = 17$). Similarly, an estimate of the number of cells fusing can be obtained by calculating the ratio of giant to single cell areas. An estimate of the amount of plasma membrane surface lost in fusion

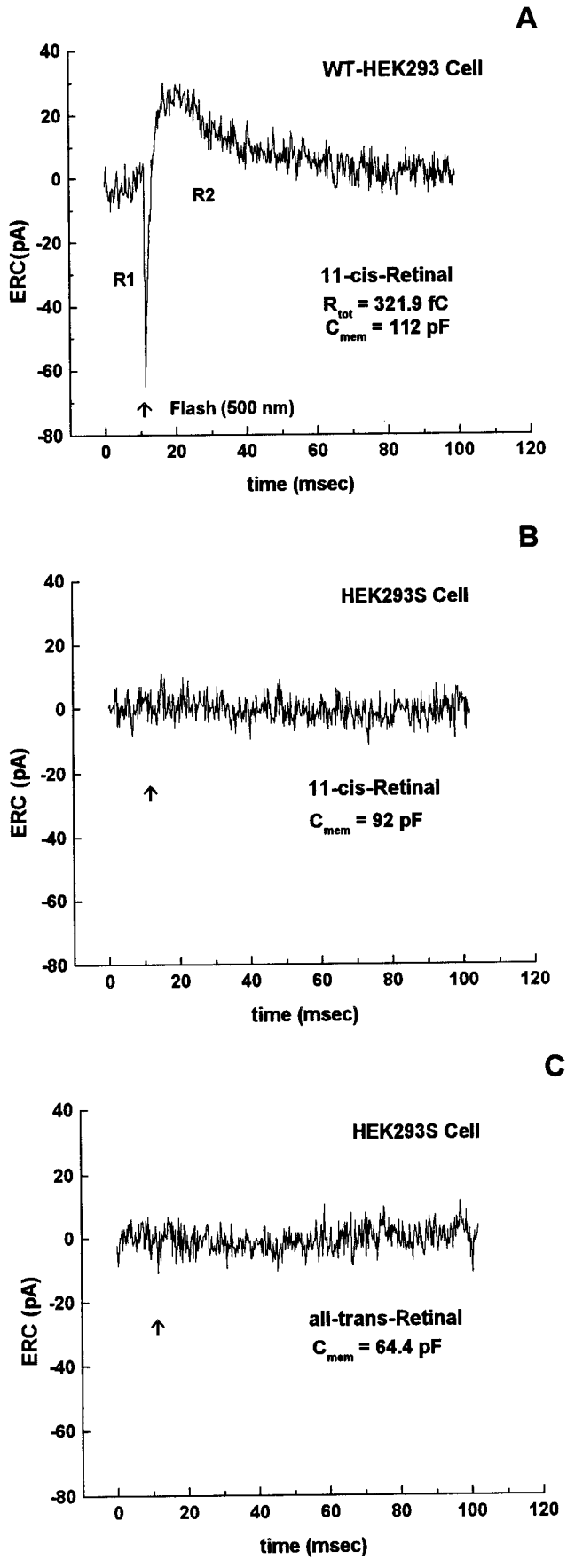

(% Lost = 1 − No. of Cells Fusing (Area)/No. of Cells Fusing (Volume)) can then be obtained. The amount lost was found to be ~40% (mean ± SE: 37.9 ± 5.6%, n = 17). Kersting et al. (1989) found 70% of the plasma membrane was lost during polyethylene glycol fusion of renal cells. Using the average fraction of membrane lost, the number of cells fusing and the opsin quantum offered by each cell, the rhodopsin concentration in fused giant cells was found to be surprisingly constant at ~2.4 μM. A similar value (0.6 μM) is found by using the slope of the fitted regression line (0.00875 ± 0.0017 SD pC/pl) and a unitary charge of 0.15e/R*. Unfortunately, the concentration of rhodopsin in the fused giant cells is below the limits of detection by microspectrophotometry (0.001 O.D.) (MacNichol, 1978). Since the concentration of opsin in fused and single cells appears to be a reliable and stable parameter, the slope of the charge versus cell volume regression line could be used to estimate the unitary charge motion (e.g., of a mutant pigment).

Light-activated charge motions require the presence of regenerated rhodopsin

ERC currents were seen upon flash photolysis only in cells that expressed opsin and were regenerated with chromophore. Control HEK293S cells that do not express opsin were also fused and regenerated with both 11-*cis*-retinal or all-*trans*-retinal and tested for ERC signals. It has not been possible to elicit ERC signals in numerous (n = 26) untransfected HEK293S cells of various fused sizes (22–92 pF) whether regenerated with 11-*cis*-retinal or all-*trans*-retinal (Fig. 6). In preliminary experiments ERCs were also not found in opsin expressing cells that were not regenerated with chromophore. These controls indicated that ERCs recorded from cells expressing opsin do not result from photolysis of nonspecific Schiff bases formed by reaction of retinaldehydes with amine side chains of membrane proteins (e.g., lysine residues) or lipids (e.g., phosphatidyl ethanolamine). Nor do they result from photolysis of membrane-oriented chromophores or from flash artifacts given the advanced design of the flash delivery system (Sullivan, 1998). The recording of ERCs requires the presence of high membrane densities of opsin and the regeneration with chromophore. These data provide strong evidence that the ERC signal results from photon activation of regenerated rhodopsin.

To test whether rhodopsin activation causes the ERC the spectral sensitivity of the signal in fused giant cells was

FIGURE 6 Flash photolysis of transfected and control cells. (*A*) A representative ERC (first 500-nm flash after primary regeneration in standard FAF-BSA solution containing 11-*cis*-retinal) is shown for a large giant WT-HEK293 cell (112 pF). (*B*) A representative recording testing for ERCs in untransfected HEK293S cells (22–92 pF) regenerated with 11-*cis*-retinal. (*C*) Recording from an untransfected HEK293S cell regenerated with all-*trans*-retinal. In all panels the 500-nm flash was given 10 ms into the record.

measured. Three-cavity 70-nm bandpass filters were used to deliver intense flashes. Signals were acquired after spontaneous regeneration for several reasons. First, after spontaneous regeneration, the R_2 component occurred in isolation and allowed direct measurement of charge flow associated with the millisecond-order states of rhodopsin activation. Second, the R_2 signal recovered over several spontaneous regeneration cycles in the dark and permitted the collection of the large amount of ERC data needed to construct an action spectrum from a single cell. This would not have been possible if recordings were obtained only from cells during the first flash series, when both R_1 and R_2 were present, because multiple cells would have been necessary. Third, the R_2 signal was larger after R_1 was lost on the first extinction and this allowed consistent ERC acquisition at good SNR. Finally, studies of the R_2 signal in isolation allowed a preliminary investigation of whether the visual pigment was substantially changed between primary and secondary (spontaneous regeneration) extinction cycles. However, the primary source of the R_1 signal, and its loss between primary and secondary bleach cycles remains to be understood. Fig. 7 shows ERCs obtained on the first flash after regeneration at four different wavelengths in a single fused cell. Small signals were seen at 350 nm in this large fused giant cell, but were absent from smaller cells because of lower SNR. Also, 350-nm flash intensities were the weakest of the wavelength series (see Methods). Large ERC signals were seen at both 430 nm and 500 nm, whereas signals at 570 nm were smaller. These responses were consistent with the ERC resulting from photon absorption by a rhodopsin photopigment with different relative sensitivities in the visible and near-UV (see Fig. 1). To test the

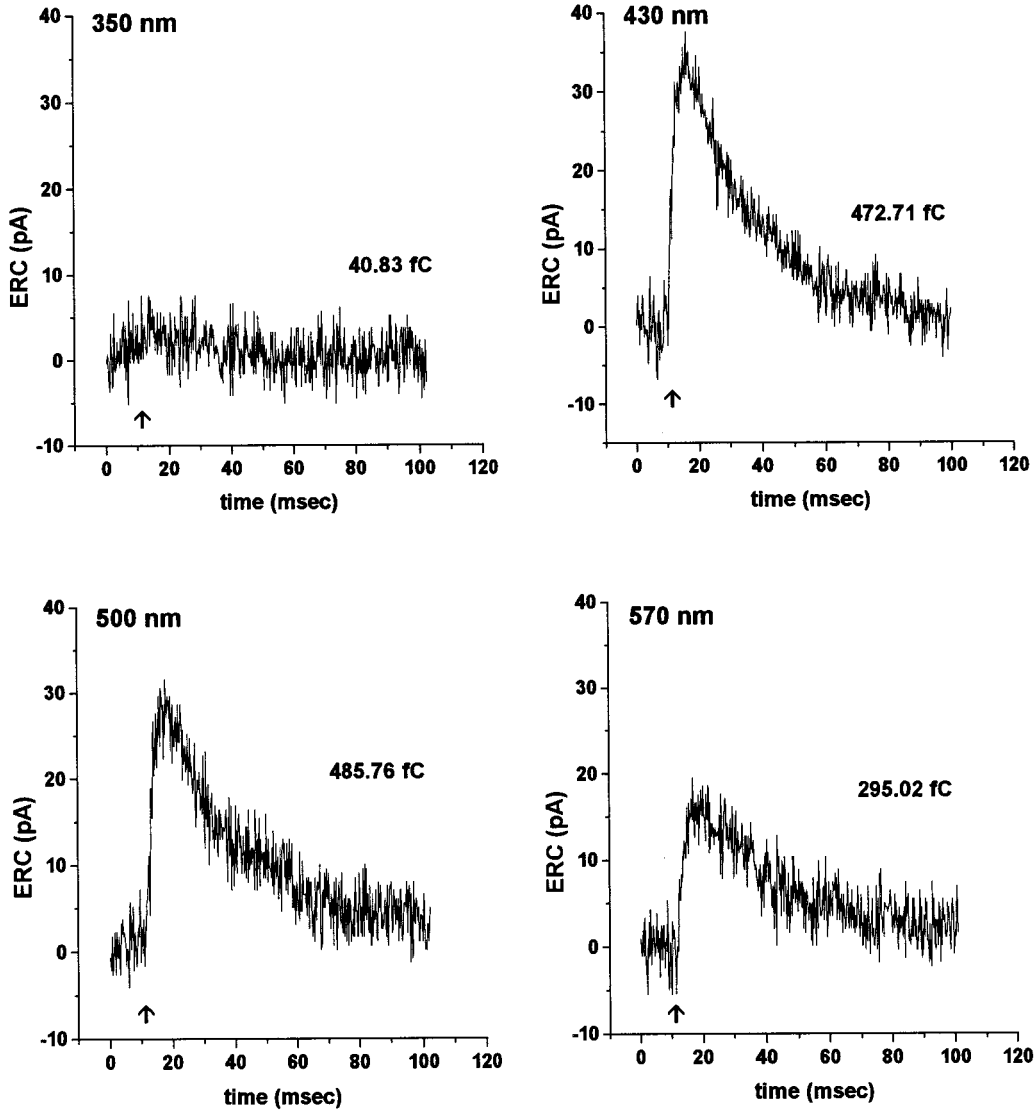

FIGURE 7 Spectral sensitivity of WT ERC waveforms. ERC waveforms on the first flash at four different wavelengths in a single fused giant cell (68 pF). All signals were obtained after 10 min of dark adaptation after an earlier extinction, which is why no R_1 signals are present. Flash intensities at different wavelengths were as stated in Methods. Multiplicative scale factors to compensate for differences in photon delivery were: 5.26 (350 nm), 1.14 (430 nm), 1.00 (500 nm), and 1.20 (570 nm).

relative sensitivity of different wavelengths of stimulation compared to 500 nm, a series of flashes were given at 430, 570, or 350 nm to extinguish the ERC into whole-cell noise at that respective wavelength. A flash was then given at 500 nm to test for residual charge motion from unbleached rhodopsin. Fig. 8 shows responses at 350 nm (1 flash), 430 nm (3 flashes), and 570 nm (3 flashes) followed by a single probe flash at 500 nm. Successive flashes promote progressive extinction of charge motion measured with the following flash. In each case the 500-nm flash resulted in more ERC charge motion in comparison to the last extinction flash at the test wavelength. Responses to the 500-nm probe flash following 350- and 570-nm extinguishing flashes were considerably larger than following 430 nm flashes. This indicated that 350- and 570-nm flashes did not extinguish available rhodopsin in the cell as well as at 430 nm, consistent with absorption properties of human rhodopsin (Fig. 1).

To obtain an action spectrum for the ERC response of WT rhodopsin, successive flashes at a given wavelength were given rapidly to extinguish the ERC into whole-cell noise. A constant criterion period of dark adaptation of 10 min allowed for rhodopsin regeneration, and ERCs were then obtained and extinguished at the next wavelength. At each wavelength the ERC currents from each flash were integrated versus time to obtain the charge motions for each signal (Q_i). The individual Q_i values were then summed to yield the total charge motion (Q_∞). Q_∞ was then multiplicatively scaled by a ratio of photon densities to reflect the differences in stimulus intensities with the different filters. Assuming linearity of response to stimulus, an equal-photon action spectrum was measured. To statistically compare spectral sensitivity data of cells differing in size and rhodopsin content, each action spectrum was normalized by dividing by the largest value of Q_∞ for each cell. Fig. 9 shows the mean action spectrum ($\pm$SE) obtained from five giant cells. Action spectra data were fit with a symmetrical Voigt function, which peaked at 479 nm. When the Voigt function was vertically scaled by varying the amplitude and offset functions (but not the center wavelength or width parameters) and then used as an overlay to the absorbance spectrum of WT human rhodopsin purified from WT-HEK293 cells (Fig. 1), the fitted ERC action spectrum is broader than the absorption of the pigment itself (data not shown). This was not surprising, however, given that broadband (70 nm) stimuli would contribute to broadening of the action spectrum. The peak of the ERC action spectrum is consistent with a human rod rhodopsin (493 nm, see Fig. 1) and suggests that 11-*cis*-retinal regenerated a normal visual pigment during spontaneous regeneration in the dark. Further work will be necessary to determine whether other spectral intermediates such as Meta-III$_{465}$, M$_{470}$, or photoegenerated isorhodopsin$_{485}$ make any contribution to the action spectrum of ERC charge motions. Preliminary observations demonstrated that ERCs remain recordable when 10 mM hydroxylamine in E-1 buffer was perfused outside giant cells. This makes the contribution to the ERC action spectrum of hydroxylamine-sensitive states, Meta-III, or M$_{470}$, highly unlikely.

ERC R_2 relaxation kinetics suggest multiple electrical states during biochemical activation

The ERC is a complex electrical signal known to relate to state-dependent charge motions during rhodopsin activation. Fig. 10, *A* and *B* show ERC responses to intense 500-nm flashes from two fused giant cells (second regeneration). The output of the joulemeter, which integrates the flash impulse energy measured by the photodiode, showed that the effective step of light energy delivered to the cell is considerably faster than the response time of the setup. Outward charge flow commenced with the recording of the flash stimulus and the peak ERC R_2 current occurred a few

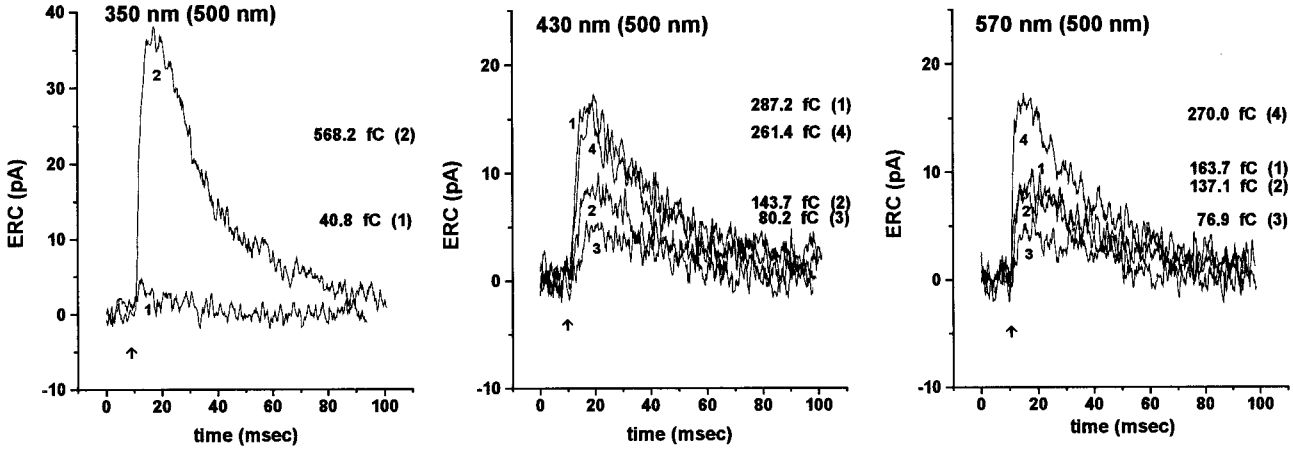

FIGURE 8 Efficiency of bleaching at different wavelengths. An extinguishing flash series was delivered at 350 nm, 430 nm, and 500 nm, followed by a single probe flash at 500 nm. When signals are at or near extinction at other wavelengths, stimulation at 500 nm (near peak absorption) is able to elicit large ERC signals. Traces were smoothed by adjacent point (5) averaging so curves could be more readily compared.

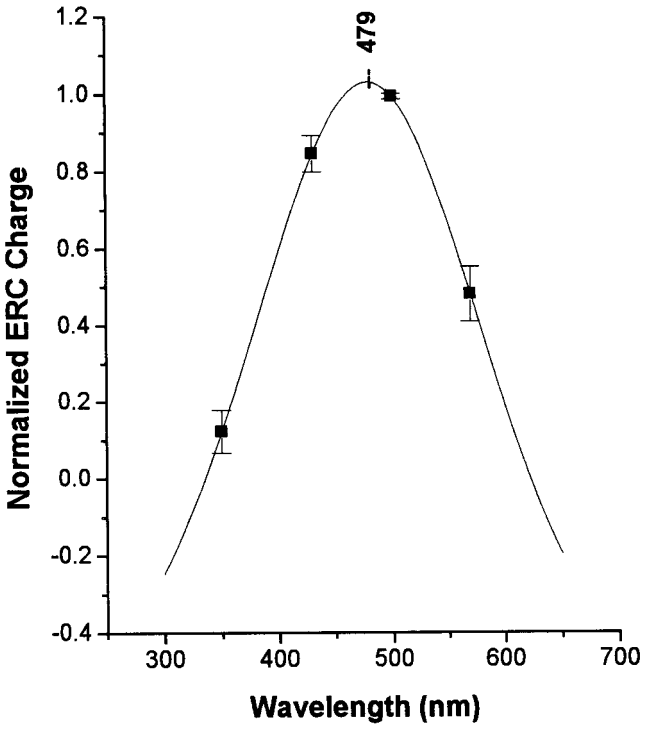

FIGURE 9 Action spectrum of WT ERC response. Action spectrum of Q_∞ versus wavelength for five fused WT-HEK293 cells regenerated with 11-*cis*-retinal in FAF-BSA solution. Holding potential was 0 mV in four cells and +30 mV in one cell, but the quality of the action spectra was not different. Q_∞ values were obtained from regenerated cells that had previously been extinguished and allowed to dark-adapt for 10 min. Where multiple extinguishing series were given at a particular wavelength the Q_∞ value at that wavelength was taken as the average across the series for a given cell. For each cell the Q_∞ values were scaled for relative intensity with respect to 500 nm such that the action spectra reflect equal numbers of photons at each wavelength. The mean (±SE) Q_∞ values are shown for the five cells and a parametrized Voigt function (see Methods) was fit to the mean data points where the fitted peak wavelength (x_c) was 479.0 nm, and the Gaussian (w_G) and Lorentzian (w_L) peak widths were 191.08 nm and 103.07 nm, respectively. There was essentially zero error in fitting the Voigt function to the mean data points.

milliseconds after the flash. To begin to investigate the state complexity of the ERC signal an analysis of the relaxation kinetics of the R_2 charge motion (after the peak of R_2) was conducted, since this signal was temporally well-resolved and correlates with major biochemical conformation changes in rhodopsin. R_2 relaxation kinetics may be a useful parameter to quantitatively compare WT and mutant rhodopsins in ERC structure-function studies. The R_2 relaxation from peak current is complex and a fast early phase and a slow late phase are appreciated. In larger ERC signals seen on the first few flashes of a given series it was necessary to fit a function of the sum of two exponentials by nonlinear least-squares minimization. Single exponentials were typically required in cells with smaller R_2 signals or near extinction of the ERC signal in a flash series on larger cells, and likely reflects the lower SNR of the ERC when rhodopsin is nearly bleached. Fitted functions are shown overlaying the two R_2 signals in Fig. 10. Residuals were largely, but typically not completely, eliminated by the fittings and in some cells a very slow "stretch" relaxation was noted. The parameter values, errors, and reliability of fitting the time constants (τ_a and τ_b) are shown and are representative of the quality of least-squares fitting in the ensemble of signals analyzed (see below). These data suggest that there are a minimum of at least two to three distinct electrically active states in the WT R_2 relaxation at room temperature.

Although the amount of ERC charge is dependent upon cell size, it was unclear how the kinetics of charge motion would be affected by cell size. This will be important for structure-function studies of the R_2 signal, which is concurrent with the major phases of conformational changes of rhodopsin to the biochemically active intermediates. Therefore, it was determined whether R_2 relaxation scaled with the rate of charging of C_{mem} in giant cells. In Fig. 11 the capacitative charging time constant of a given cell (τ_{cap}) was plotted with respect to separable ERC R_2 relaxation time constants (τ_a, τ_b) for a set of cells ($n = 17$) with a broad range of cell sizes (29.9–127.2 pF). A large number of ERC waveforms were fitted ($n = 53$). In those cells where two exponentials were required to adequately fit τ_{cap}, the more heavily weighted slower τ_{cap} value was used in the analysis. Fig. 11 *A* shows the entire data set where each time constant in the ensemble (τ_a or τ_b) was related to the respective τ_{cap}. ERC time constants were distributed across the range of τ_{cap} values measured. A linear regression showed no statistically reliable correlation between the ERC relaxation constants and capacitative charging. When τ_a and τ_b values were examined separately (Fig. 11, *B* and *C*) there also was no reliable linear correlation with τ_{cap}. However, in the τ_a versus τ_{cap} data (Fig. 11 *B*) there appeared to be a positively sloping trend in the shortest τ_a time constants as τ_{cap} increased. A histogram for the isolated τ_a data set was fit to an unrestricted single Gaussian function, which demonstrated a prominent peak centered around 4.4 ms (Fig. 11 *D*). The histogram for τ_a was skewed by many larger τ_a values that were not fit by the Gaussian; τ_a values >9.0 ms were not embraced by the envelope of the Gaussian function. When these were excluded from the τ_a set a reliable regression line could be fit to the data, although the correlation coefficient was somewhat low due to existing scatter of points around the fitted line (Fig. 11 *E*). This analysis demonstrated that the relaxation of the WT R_2 signal was essentially independent of τ_{cap} or cell size, except perhaps for the fastest τ_a values when they overlap with estimates for capacitative charging time (see Methods). This is consistent with the identification of the ERC as a capacitative current. Moreover, given this analysis, the kinetics of R_2 could be compared between mutant and WT pigments, especially when fused giant cells of uniform size are used for ERC recordings.

The time to reach R_2 peak current (τ_{peak}) was measured from the flash stimulus for each ERC signal in the ensemble ($n = 53$). ERC signals were first smoothed by adjacent point

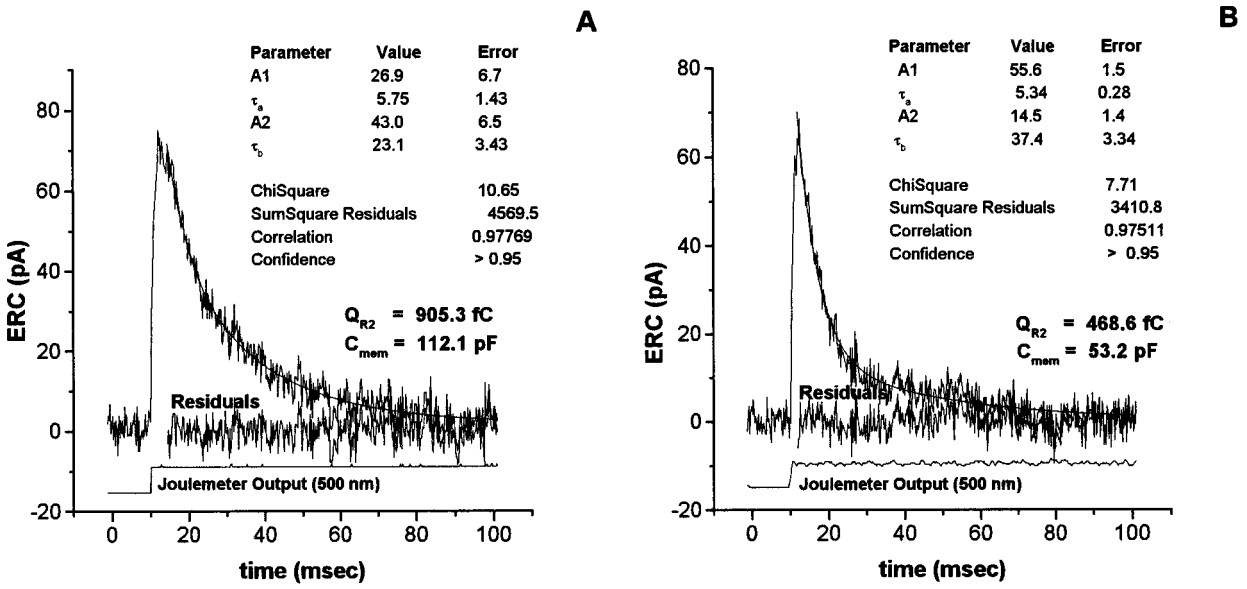

FIGURE 10 R_2 relaxation kinetics demonstrate multiple electrical states. The time course of the R_2 relaxation (after the peak of R_2) was fit with single, double, and triple exponential models (see Methods). The fitting range began at a time (t_o) just beyond the peak of the R_2 signal. Time constants were taken from the most reliable model. ERCs from two fused giant WT-HEK293 cells are shown (Fig. 10, *A* and *B*). The ERC in Fig 10 *A* was from a cell held at +30 mV and the ERC in Fig. 10 *B* was from a cell held at 0 mV. The joulemeter output signal shows the integrated response (unit step) of the photodiode to the flash impulse stimulus (14 μs). The R_2 phase of the ERC rises rapidly to a peak upon flash stimulation. In these large ERCs double exponential functions provided reliable fits to the R_2 relaxation. Residuals are shown below the ERC signals. The respective time constants (τ_a, τ_b) and reliability characteristics of the fit are shown (*inset*).

averaging (5 point) to decrease noise and allow reliable estimation of the time between the flash and the peak of R_2 current. Flash stimulation time was measured from the time of initial rise of the photodiode signal. Peak R_2 times of those ERCs ($n = 12$) that had R_1 signals ("R_1") or those without R_1 signals ($n = 42$) ("R_2") were separated from the set of all peak times ("Total") for independent analysis. Table 1 shows the mean, variance, SD, and SE for the three distributions. One-way analysis-of-variance showed that the mean of the "R_2" subset was not different from the "Total" data set. However, the mean of the "R_1" subset was significantly different from "Total," even though the total set contained the R_1 subset. This suggested that τ_{peak} of ERCs with R_1 signals was different from those that only had the R_2 phase. The mean τ_{peak} values of these respective subsets were significantly different. Since the mean "R_1" τ_{peak} was 6.9 ms and the mean "R_2 τ_{peak} was 3.6 ms, this analysis indicated that the presence of the R_1 signal delays the transition to the R_2 generating states. This may suggest additional electrical state complexity on the path to R* formation.

The τ_{peak} values depend upon τ_{cap} as shown in the scatter plots for ERC signals that had both R_1 and R_2 signals (Fig. 12 *A*) and those that had only R_2 signals (Fig. 12 *B*). In both cases reliable regression lines were fit to the data. This suggests that quantitative comparisons of τ_{peak} between WT and mutant pigments should be scaled to the size of the cell (e.g., pF).

DISCUSSION

Rhodopsin is the visual pigment underlying the ERC signals in WT-HEK293 cells

There are several reasons for concluding that the flash-activated whole-cell currents are the ERC of 11-*cis*-retinal-regenerated human rhodopsin. First, the ERC action spectrum, even generated with broad stimulus bandwidth, is consistent with a human rod rhodopsin photopigment. Second, ERC signals were never found in HEK293S cells that are the untransfected parent line used to make WT-HEK293. Since the parent line does not express opsin and is otherwise identical to WT-HEK293 cells, ERC signals must originate as a consequence of the presence of expressed and 11-*cis*-retinal-regenerated opsin. Third, the signal shape and kinetics are similar to ERCs recorded from rod or cone photoreceptors in previous studies using similar ranges of light intensities (Hestrin and Korenbrot, 1990; Makino et al., 1991). The τ_a parameter representing the fast R_2 relaxation is nearly the same as the mean value recorded in rod photoreceptors (3.2 ms, Makino et al., 1991) and the τ_{peak} of R_2 is also similar (1.9 $\pm$ 0.3 ms, Makino et al., 1991). Fourth, the signal progressively decreases to extinction with sequential flashes consistent with the irreversible bleaching of a vertebrate rhodopsin similar to previous photoreceptor ERC studies (Hestrin and Korenbrot, 1990; Makino et al., 1991). Fifth, the signal can be regenerated with 11-*cis*-retinal consistent with an opsin apoprotein with a ligand

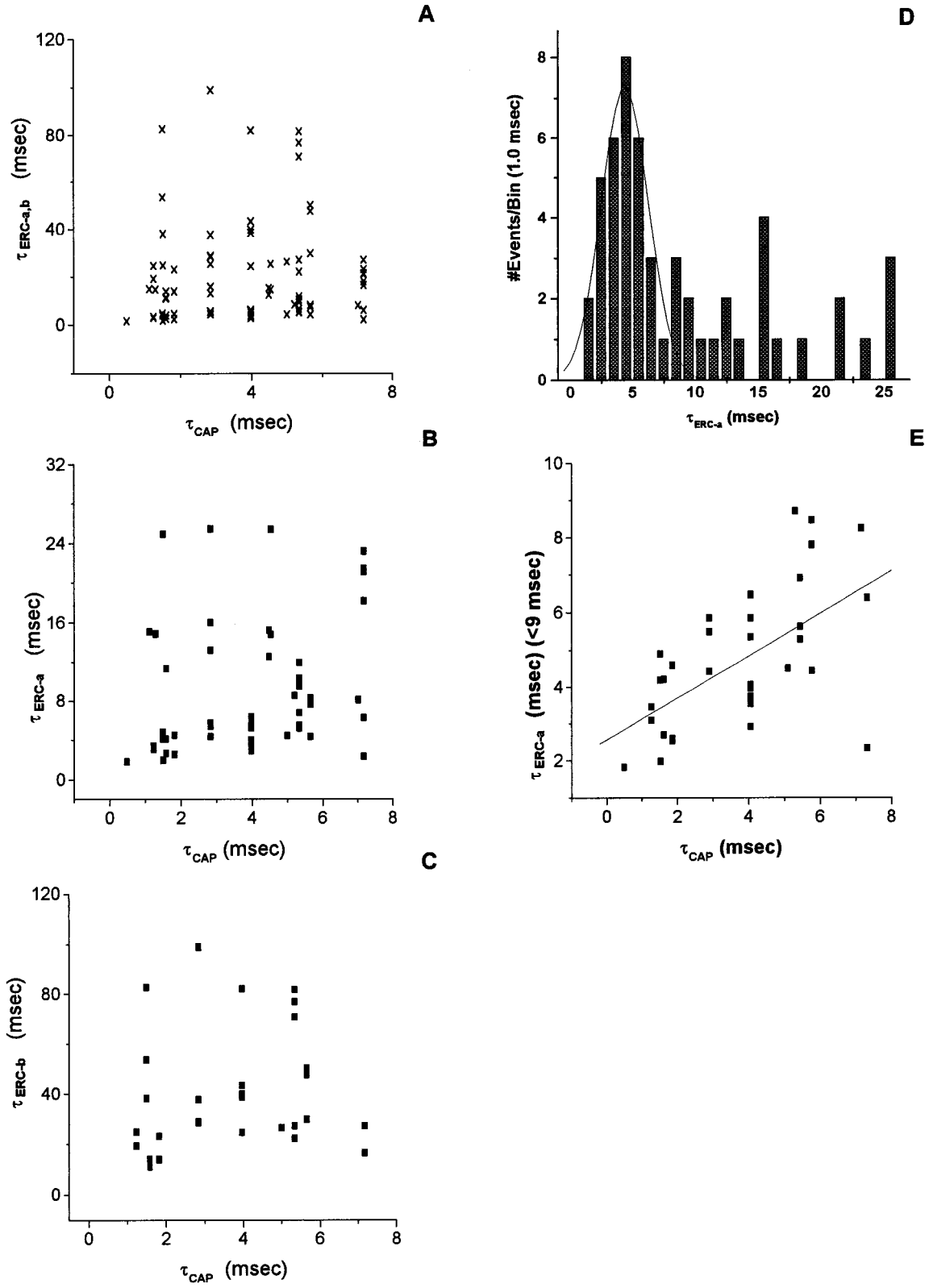

FIGURE 11 R_2 relaxation kinetics are independent of cell capacitance. Relaxation kinetics beyond the R_2 peak were fit by single, double, and triple multiexponential functions for a large set of cells ($n = 17$ cells, 53 ERC waveforms). Both primary and secondary regenerated signals were pooled. The most reliable fits were used to determine the time constants [τ_a (fast), τ_b (slower)] for each signal. Triple exponentials occasionally fit the data but the parameter set was more reliably represented with only two exponentials. Cellular capacitative time constants (τ_{cap}) were determined by fitting a single or double exponential to the decay of the cellular capacitative current (+20 mV test pulse). In those instances where two exponentials were required the slower τ_{cap} was used in the scatter plots. In one of the cells the holding potential was +30 mV but the fits from the ERC waveforms from this cell (8 ERCs) were

TABLE 1 Statistics on time-to-peak of the R_2 signal

τ_{peak}	Mean*	Variance	SD	SE	*n*
"Total"	4.34	5.34	2.31	0.31	54
"R_1"	6.94	4.39	2.09	0.60	12
"R_2"	3.60	3.19	1.79	0.28	42

*One-way analysis of variance indicated that the "R_1" mean was significantly different ($p < 0.05$) from the "Total" mean (*F*-statistic 12.77, $p =$ 6.8E-4). The "R_1" mean was significantly different from the "R_2" mean (*F*-statistic 30.145, $p =$ 1.21E-6). The "R_2" mean was not significantly different from the "Total" mean (*F*-statistic 2.94, $p = 0.09$). See text for further explanation.

binding pocket accessible to chromophore whether it originates from either exogenous or endogenous sources (Knowles and Dartnall, 1977). In fact, Makino et al. (1991) also saw spontaneous regenerations of ERCs in intact photoreceptors after they used liposomes to deliver chromophore. Sixth, the signal kinetics show no apparent change at different wavelengths consistent with the temporal invariance of the ERC (Makino et al., 1991). Invariance results because the conformation or chemical changes (measured electrically) are only triggered by light but are not directly dependent upon the stimulation wavelength. Signal shape is the same regardless of the energy of the photon that excited the pigment. Seventh, charge magnitudes and polarity were similar to ERC signals resulting from rhodopsin activation in amphibian rod photoreceptors (Hestrin and Korenbrot, 1990; Makino et al., 1991) which have plasma membrane rhodopsin levels ($1.2–1.9 \times 10^7$ molecules) comparable to single and fused WT-HEK293 cells (6×10^6-7×10^7). This indicated that the unitary charge motions (0.15 e/R*) resulted from a conserved property of the rhodopsin protein and not the environment in which it is situated. Eighth, since R_2 polarity is outward going in both photoreceptors and in WT-HEK293 cells, the opsin expressed in these cells must be oriented outside-out (intradiskal face outward). Finally, although there are sufficient photons to activate all rhodopsins in the cell on the first flash at 500 nm, several flashes are necessary to extinguish the signal following stimulation in the major absorption band. This is consistent with the fact that only 50% of rhodopsin can be bleached in a single flash due to second photon resorptions from short-lived intermediates (e.g., bathorhodopsin, lumirhodopsin) with lifetimes overlapping the flash duration (Williams, 1964, 1965). This suggests that the expressed rhodopsin also has the capacity for photoregeneration.

These studies utilized a physiologically stable cell line programmed to constitutively express WT human opsin to high levels. It is anticipated that an otherwise identical approach will be very effective in studying electrical processes associated with activation of site-specific mutants of rhodopsin. This will require high-level expression of mutant rhodopsin, such as in stable cell lines.

The ERC demonstrates multiple electrically active states during rhodopsin activation

In WT-HEK293 cells the kinetically unresolved inward R_1 current precedes the larger and outward R_2 signal in a similar relationship to that occurring in photoreceptors. The time from the flash to the peak of the R_2 signal (τ_{peak}) was ~7 ms, indicating distinct conformational transitions from the early R_1 charge states to the R_2 generating states and an alteration in the polarity of molecular charge flow. The R_2 signal relaxation from its peak is complex and typically required the sum of two exponentials to fit the kinetics of individual ERC waveforms. While it was not our intent to develop mechanistic models in this initial work, these findings indicated that at least two or three unique charge mobilizing states occur during the R_2 relaxation concurrent with the critical period of biochemical activation to R*. This assumes that each state undergoes memoryless (Markovian) transitions with unique exponentially distributed lifetimes. Makino et al. (1991) found a single exponential fit adequate for the R_2 relaxation at room temperature (τ_{ERC} 3.2 ± 0.8 ms) when fitting individual ERC waveforms from the rod photoreceptor. Similarly, Ebrey (1968) found a relaxation time of 2 ms at room temperature for the lifetime of Meta-I (i.e., Meta-II formation) in the rat eye using ERP techniques. The ERP R_2 relaxation in rod photoreceptors attached to membrane filters was ~10 ms at room temperature (Lindau and Ruppel, 1983). The fastest time constant (≈5 ms) of R_2 decay in WT human rod rhodopsin photolyzed in WT-HEK293 giant cells was consistent with former studies. This value is also consistent with the expected rate of Schiff base deprotonation and the formation of Meta-II_a from Meta-I at room temperature of a few milliseconds (Parkes and Liebman, 1984). However, whether the fast R_2 charge motion reports Schiff base proton transfer remains to be determined in future experiments. Suggestions were made in previous studies that the R_2 signal reflected Schiff base deprotonation in voltage-dependent dye and ERP measurements on rod disks or photore-

not distinguished in the distributions plotted below. All other ERCs were obtained at 0 mV holding potential. (*A*) Scatter plot of all $\tau_{a,b}$ fits versus τ_{cap} (mean ± SE: 22.4 ± 3.1). A reliable regression line could not be fit through the data. (*B*) Scatter plot for the τ_a values (mean ± SE: 9.1 ± 0.95 ms, $n =$ 53). No reliable regression line could be fit through the points. (*C*) Scatter plot for the τ_b values (mean ± SD: 45.1 ± 6.3 ms, $n = 31$). No dependence upon cell capacitance was identified. (*D*) A histogram of all τ_a values is skewed but is fit with a single (unrestricted) Gaussian function that is centered around 4.4 ± 1.9 ms. Almost all the weight under this Gaussian is represented by τ_a values ≤9.0 ms. Values greater than this were then excluded to yield a reduced τ_a set (mean ± SE: 4.71 ± 0.32 ms, $n = 34$). (*E*) The regression line found to fit the τ_a values within the single Gaussian distribution envelope had a shallow slope (0.569 ± 0.139) and a low correlation coefficient (0.59).

ceptors (Bennett, 1980b; Lindau and Ruppel, 1985). The slower time constants that were recorded in R_2 decay (10–40 ms) in this study could be consistent with the expected rate of proton uptake into the cytoplasmic face of rhodopsin (Arnis and Hofmann, 1993). These time constants are also consistent with spin resonance probe measurements of proton uptake signals or complex α-helical conformational changes near the cytoplasmic face during R* formation (Cafiso and Hubbell, 1980; Farahbakhsh et al., 1993, 1995; Altenbach et al., 1996; Han et al., 1996). Further experiments will be necessary to determine whether these electrical transitions represent the stated processes.

More complex ERC signals were recorded from giant cells, which typically contain more absolute plasma membrane rhodopsin than is found in intact giant amphibian rod photoreceptors. This suggests that the SNR improvements obtained by recording ERCs in giant cells allowed discovery of a greater complexity in the unicellular ERC signal. Signal shape is similar in small and large cells, suggesting some degree of scaling with the amount of rhodopsin present. It should also be mentioned that the separable time constants, the variability in fitting exponential functions to R_2 decay, and the remaining residuals are also consistent with an ERP study (Lindau and Ruppel, 1983) where power laws were necessary to fit the complex R_2 relaxation kinetics. A major conclusion was that a multitude of electrically active states with similar activation energies occurred during Meta-II formation and lifetime. Similarly, Thorgeirsson et al. (1993) and Arnis and Hofmann (1993) have recently demonstrated the presence of multiple conformational states concurrent with Meta-II formation.

The expression ERC as a new approach to study rhodopsin activation in a unicellular expression system: signal reliability and technical limitations

An electrophysiological assay was developed to record electrical charge states concurrent with rhodopsin activation by flash photolysis in a simple unicellular expression system. The assay has the capacity to completely resolve the kinetics of state changes during the R_2 phase of the ERC. The temporal scale of R_2 correlates with critical transformations in rhodopsin conformation to the biochemically active R* state, which are now thought to be largely electrostatic in nature (Shieh et al., 1997). The sensitivity of the method is such that charge motions were recorded from about a picoram of expressed WT human opsin regenerated with native chromophore. The significant technical advances, which permitted not only larger ERC signals with better SNR but also the surprising "visual cycling," were the combination of fusion of stably expressing cell lines and the efficient rhodopsin regeneration technique with albumin as a delivery vehicle (McDowell, 1993). Sheets et al. (1996) were the first group to use the HEK293 expression system to study ionic channel gating currents of voltage-dependent sodium channels by transfecting already fused cells with plasmids.

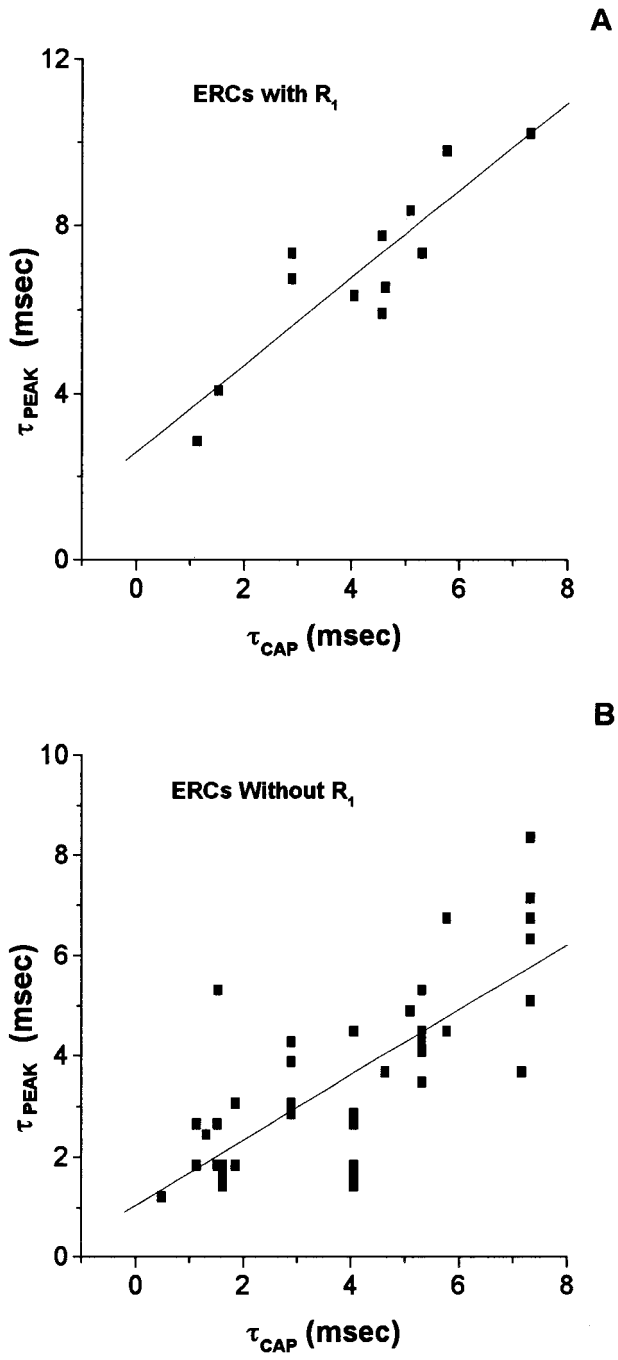

FIGURE 12 Time to peak of R_2 is dependent upon cellular capacitative charging. τ_{peak} for each was waveform was plotted versus τ_{cap} for ERC signals that had both R_1 and R_2 components (*A*) ($n = 12$) and those that had only R_2 components (*B*) ($n = 42$). Regression lines were fit to the data. For (*A*): ($\tau_{peak} = 2.61 + 1.04 \cdot \tau_{cap}$; slope 1.04 ± 0.18, $R = 0.88$, $p < 0.001$). For (*B*): ($\tau_{peak} = 1.06 + 0.65 \cdot \tau_{cap}$; slope 0.65 ± 0.09, $R = 0.75$, $p < 0.0001$).

Since an estimate of the density of channels can be obtained by ionic current measurements, it was easy to select for cells that had large gating currents. Clearly, one cannot do this for rhodopsin, so, to guarantee uniform rhodopsin density, cells that were already stably transfected to express high and

uniform levels of normal human opsin were fused in order to ensure that no untransfected cells were contributing to giant cell formation.

These experiments establish the use of single and fused cell ERCs as a time-resolved assay of human rhodopsin activation in a physiologically intact heterologous expression system. The levels of ERC signal are consistent with the amount of rhodopsin/cell determined spectroscopically and indicate that essentially all of the WT opsin is expressed to the plasma membrane. The expressed opsin regenerates efficiently with 11-*cis*-retinal without loss of cell vitality, and can be conveniently "cycled" from an endogenous source of chromophore built up in the cell by prior loading. Similar spontaneous regeneration effects occur in isolated photoreceptors that were efficiently regenerated with 11-*cis*-retinal (Knowles and Dartnall, 1977; Jones et al., 1989; Makino et al., 1991). High-fidelity ERC data can be obtained with ion channel blockade by permeant ion replacement, and experiments lasting >2 h have been conducted on some single giant cells. Given that the amount of human rhodopsin regenerated in a single cell is on the order of a picogram, the ERC as a time-resolved assay has 10^7-10^8-fold greater sensitivity for studying rhodopsin activation, for example, in comparison to time-resolved ESR or absorption spectroscopy, respectively (Jager et al., 1997). Time-resolved absorption (or FTIR) spectroscopic studies of expressed rhodopsin pigments require milligrams of regenerated pigment, whereas time-resolved ESR requires hundreds of micrograms but is limited to millisecond time resolution. The ERC requires picograms of rhodopsin and only single cells, and at this point has submillisecond time resolution. This achievement results from the application of modern electrophysiological techniques to a problem that has been previously studied mostly with spectroscopic tools.

Parameter reliability is an important factor to consider in the development of a new biophysical approach. Most parameters in ERC studies can be measured reliably without knowing the amount of rhodopsin present in each cell. This includes, for example, kinetic analysis, action spectra determination, and bleaching photosensitivity experiments. Good estimates of rhodopsin concentration are essential only in those ERC experiments where the parameter being evaluated is an extensive variable. Extensive parameters such as the unitary charge motion or thermodynamic properties of charge states (e.g., ΔH) do require knowledge of the amount of opsin present (in moles). The analysis of ERC charge (Q_∞) from single cells led to a statistical estimate of the amount of plasma membrane rhodopsin which was comparable to that measured by detergent extraction and immunoaffinity purification from the same WT-HEK293 cell line. To make this comparison the effective charge motion of WT rhodopsin in the expression system was assumed to be the same as in photoreceptors (0.15 e/R*). In fact, the unitary charge motion was the only parameter assumed from the literature for ERC charge analysis in these experiments. This was a reasonable assumption given that the unitary molecular charge motion of rhodopsin activation is a conserved feature of rod or cone rhodopsins from different organisms (Hodgkin and O'Bryan, 1977; Govardovskii, 1979; Drachev et al., 1981; Hochstrate et al., 1986; Makino et al., 1991). The evolutionary conservation of unitary charge motion may indicate the importance of electrical events in the late phases of visual pigment activation. However, as found in single cell ERC experiments, one can also obtain the unitary charge motion a priori from Q_∞ if one has an estimate of the fraction of plasma membrane rhodopsin and one knows the mean number of rhodopsin molecules per single cell from spectrophotometry. The unitary charge motion for WT rhodopsin was estimated to be 0.186e/R* in single-cell experiments and approximates that recorded in photoreceptors. It was essential that a stably expressing WT cell line was used which showed little, if any, variability in the immunocytochemical pattern of opsin staining over time because the opsin is expressed from integrated transgenes. For those opsin mutants that partition only partially in the plasma membrane, rhodopsin should be quantified in isolated plasma membrane fractions from single cells.

To obtain estimates of the amount of rhodopsin in giant cells of different sizes is more difficult. It will first require measurement of the rhodopsin concentration in the plasma membrane of stably expressing single-cell populations. Since polyethylene glycol cell fusion is an isovolumic process that maintains the surface/volume ratio (Kersting et al., 1989), one can make the experimentally testable assumption that the concentration of rhodopsin in fused giant cells of various sizes is the same as that in the plasma membrane of single cells. The data in Fig. 5 *C* provide support for this assumption. With an estimate of the concentration one can measure Q_∞ in cells of different volumes and calculate the elementary charge motion from the inverse slope (l/C) of the Q_∞ versus volume regression line as was done in photoreceptors (Makino et al., 1991):

$$e/R^* = (1/C \cdot \text{moles}/1 \cdot 6.02 \times 10^{23}\ \text{molecules/mole} \cdot 1.602 \times 10^{-19} C/e)^{-1}.$$

This approach should be useful to reliably quantify charge motion parameters of mutant rhodopsins that may have different unitary charge values when compared to WT but require the fused giant cell system to obtain reliable SNR in ERC data acquisition.

The ERC assay is conducted using ultrasensitive patch clamping techniques and has time-resolution capabilities that will be limited largely by whole-cell recording technology applied to single or fused giant cells. The bandwidth of whole cell recording will depend in part upon the design of the voltage clamp apparatus and the digitization hardware (see Marty and Neher, 1983; Rae and Levis, 1984). The critical parameters for whole-cell voltage clamp recording will be the experimental variables of C_{mem} and R_{ser}. For the largest fused cells used here ($\approx$100 pF) and the smallest resistance pipettes that could be made (500 kΩ) (R_{ser} is

minimally about two times electrode resistance), the temporal limits of the voltage clamp ($R_{ser} \times C_{mem}$) would be ~100 μs without compensation and for the small signal range of ERCs at most 10 μs if compensation were used. For smaller cells the clamp response time could approach ~1–2 μs with compensation (see Marty and Neher, 1983). However, compensation could distort the ERC signal, which is a capacitative current. Thus, there appear to be distinct limits in the use of cellular electrophysiology to understand the mechanism of R_1 signal generation.

The temporal properties of light delivery are also critical in ERC recordings. The pulse duration of the xenon flash apparatus used in these experiments was ~14 μs with a risetime of ~5 μs at full capacitor charge (Sullivan, 1998). Thus to approach the limits of the voltage clamp risetime to study kinetics of fast charge motions (e.g., Meta-I formation from Lumi) one would have to deconvolve the charge motions with the flash output response. Well-resolved signals as fast as 50 μs (~4× flash duration) could be recorded in the current apparatus without kinetic deconvolution assuming that the anticipated increase in noise did not significantly compromise SNR. Another critical factor is the relationship of the flash duration to photoreversal from different states. Stimulus durations on the order of 1 ms can bleach only 50% of the existing rhodopsin in a preparation with a single flash. This results because photoregeneration of ground state(s) occurs from thermal rhodopsin intermediate states that overlap with the duration and spectral bandwidth of the flash. Our interests were predominantly associated with charge motions concurrent with the Meta-I/Meta-II equilibrium. Since Lumi is fully formed by 1 μs and Meta-I formed by 100 μs at room temperature, the flash duration of 14 μs would permit no overlap of photon delivery with the lifetime of Meta-I formation or decay. In this way the ERC components would reflect thermal state changes independent of photochemical reversal from Meta-I, which has high relative quantal efficiency (0.55) for conversion to rhodopsin (Ebrey, 1968). A brief xenon flash stimulus or a laser pulse stimulus are sufficient to record ERC signals concurrent with the Meta-I/Meta-II equilibrium.

There are also noise limitations. For example, the 0.5 GΩ feedback resistor in the patch clamp was used to record ERC signals in order to have access to C_{mem} and R_{ser} compensation in the Axopatch 1C amplifier and wider bandwidth. If one is not going to use compensation, then the 50 GΩ resistor could be used which would lead to somewhat lower noise, especially for small cells, yet be capable of providing sufficient range to record up to 200 pA ERC currents. A potential disadvantage of using fused cells was an increase in background current noise over which ERCs would be recorded. Fusion increases cell surface area and C_{mem} and was also expected to increase the numbers of both rhodopsin and plasma membrane ionic channel molecules. Increased channel number would predictably cause an increased shot current noise, especially at low frequencies (100–1000 Hz) (Marty and Neher, 1983; Rae and Levis, 1984). In order to suppress ionic current noise, solutions for both bath and pipette (intracellular) were designed to replace essentially all permeant ions (sufficient Cl^- remains from pH calibrations to operate Ag/AgCl electrodes). The clear dominant noise source during whole-cell recording between 1 and 5 kHz, however, is the series relationship of C_{mem} with the thermal voltage noise of the recording pipette (e_p) (Marty and Neher, 1983; Rae and Levis, 1984); $e_p^2 \approx 4kTR_p$, where k is Boltzmann's constant, T is absolute temperature, and R_p is pipette resistance in ohms. The dominant spectral noise density, S_m, under whole-cell recording is given by $S_m = 4\pi^2 C_{mem} e_p^2 f^2$. Since C_{mem} increases proportionally to giant cell size, the only experimental way to reduce S_m is to decrease R_p. In the giant cell ERC experiments reported here the pipettes used had a relatively low R_p (8.6 ± 0.25 MΩ) with solution I-1 in the pipette and E-1 in the bath. These pipettes permitted ERC recordings with high SNR in the described experiments. If lower noise is required in future work it should be possible to generate pipettes from Corning 8161 glass having resistances below 800 KΩ, given that 500 KΩ electrodes can be made with the same glass (Rae and Levis, 1984). These efforts should reduce the dominant form of whole-cell current noise by about an order of magnitude compared to the data reported here.

Another essential yet potentially limiting variable in ERC studies of rhodopsin activation is the expression system. Calculations indicate that levels of regenerable opsin in the plasma membrane must be quite high, on the order of ~10^6 opsins/single cell in order to achieve significant ERC signals above noise. This level is likely to be achievable for many different rod opsin mutants given levels of expression reported in COS and HEK293 cells. However, it is unlikely to be the case for mutants that fail to fold properly or traffic poorly from the Golgi apparatus to the plasma membrane or those mutants that have degenerate capacity to combine with 11-*cis*-retinal. Another relevant point here is that if the fused cell system is to be used, it is highly recommended that constitutively expressing opsin cell lines be developed such that opsin density in the plasma membrane can be somewhat predictable for those experiments (e.g., thermodynamic) where the concentration needs to be an estimable parameter. Expect the development, screening, and quantitation of stable opsin expression lines to be a process requiring months of experimental time (Sullivan and Satchwell, in press). Finally, it is important to note that the COS cell system that is often utilized for transient expression of rhodopsins has not found utility in expression of membrane proteins for low noise electrophysiology. This is presumably because the powerful overexpression makes the plasma membrane leaky, which would predictably increase thermal noise and ERC signal degradation. However, COS cells or the *ts*A201 strain of HEK293 cells might be useful for mutants that do not express well to the plasma membrane. For transient transfection experiments either very high efficiency transfection protocols can be applied to single cells before fusion or transfection of previously fused cells can be accomplished (see Sheets et al., 1996).

Future promise for the expression ERC approach

The sensitivity and bandwidth of gigaohm-seal whole-cell recording of the ERC now permits an investigation of the underlying molecular mechanism of how this signal is generated and the contribution of electrical forces to conformational activation of rhodopsin to R*. The ERC method should assist in structure-function studies of mutant rhodopsins that are difficult to express in sufficient quantities for biochemical studies, point mutations at residues known to be important for activation, or human rhodopsin mutations that cause hereditary retinal degeneration and may be altered in rapid activation processes (Sung et al., 1991). The "expression" ERC thus adds a new technical dimension for scientific exploration of the biophysical and molecular processes that control rhodopsin activation (Sullivan et al., work in progress). This method could also be well-utilized to study expressed cone rhodopsin pigments provided that plasma membrane opsin levels achieved are comparable to cone photoreceptors that generate robust ERC signals (Makino et al., 1991). Finally, this approach could be applied to any G-protein coupled receptor provided that the ligand could be presented rapidly, for example, by flash photolysis of either solubilized caged pharmacophores or covalently attached, site-directed, and light-sensitive ligands.

A major problem remaining in visual excitation is to understand how conformation changes in the rhodopsin chromophore environment propagate orthogonally across the membrane to influence the structural changes on the cytoplasmic face that permit transducin binding. Critical to this millisecond-order biochemical activation is the deprotonation of the Schiff base following a marked decrease in its pK_a (Longstaff et al., 1986). Deprotonation occurs to the $E113^-$ counterion eliciting conformation changes in the α-helices, proton uptake into the cytoplasmic face, and a molecular volume expansion of the protein consistent with a large increase in entropy (Lamola et al., 1977). The millisecond-order R_2 process moves 0.15e equivalent charges per molecule (Hodgkin and O'Bryan, 1977; Govardovskii, 1979; Hochstrate et al., 1982; Makino et al., 1991). For a positive charge this could mean a net outward movement through ~15% of the entire membrane field. The R_1 phase is a net inward charge motion of ~0.02e (Govardovskii, 1979), suggesting, for example, that a single positive charge moves ~2% through the membrane field. These charge motions in rhodopsin are, by definition, conformation-dependent currents. Ionic channel gating currents belong to this large family of protein electrical signals (Honig et al., 1986). For example, gating currents of ionic channels are critical to the underlying conformational changes that sponsor the large molecular volume increase associated with the opening of the pore. Structure-function studies using gating current assays have had a major impact on our current understanding of the molecular processes of ionic channel activation. The ERC of rhodopsin is not only curiously similar in waveform and kinetics to an ionic channel gating current, but it also is concurrent with critical electrical transformations in the membrane-oriented rhodopsin molecule during the time scale of known molecular volume changes. Thus, we speculate that the ERC is a rhodopsin gating current. It is particularly interesting that the occurrence of R_1 slows the transition to peak R_2 current and inhibits the total outward charge motion of R_2. Does the presence of R_1 indicate that a significant fraction of R_2 gating charge is stably immobilized (see Bezanilla and Stefani, 1994)? Does R_1 originate in the chromophore environment? What molecular properties create this signal and how do they control R_2? Are ERC charge motions an indirect byproduct of the conformational changes during activation or do they play a more direct role in the molecular biophysics of conformational activation? Experiments are in progress to answer these questions.

The ERC offers a unique tool to probe conformational transitions that mobilize charge in environments which absorption spectroscopy cannot probe or where spin probes cannot be placed. The ERC measures net charge displacement with respect to the membrane capacitor and its vector is largely orthogonal to the chromophore state transitions. Thus, the ERC can predictably be used as an ultrasensitive assay to study conformational changes that are orthogonal to the membrane plane. A major challenge is to design experiments to dissect what molecular processes contribute to the *net* transmembrane ERC signal during activation. Such electrically active events could include chromophore dipole reorientation, fixed charge separation, macrodipole (α-helix) movement, intramolecular proton transfer (e.g., $PSB \rightarrow SB + H^+$), and vectorial proton uptake or release from the interfacial membrane boundary solutions. All of these processes are known to be associated with conformational and chemical changes in rhodopsin that lead to the R* state.

SUMMARY AND CONCLUSIONS

In this study a novel biophysical approach was developed to study rhodopsin activation in a unicellular expression system. Rhodopsin activation was studied with submillisecond time resolution as conformation-dependent charge motions similar to ionic channel gating currents. Single living giant cells containing ~1 pg of regenerated visual pigment were used for study. Compared to other time-resolved biophysical methods applied to rhodopsins, this approach improved sensitivity seven to eight orders of magnitude. This achievement resulted from application of modern single-cell electrophysiological methods to a high-level cellular expression system for wild-type rhodopsin. Rhodopsin charge motions are commonly known as early receptor currents, and those recorded in the expression system have waveforms similar to those elicited from intact photoreceptors. The temporal scale of the slower R_2 charge motion overlaps with the kinetics of appearance of the biochemically active R* state (metarhodopsin-II) in photoreceptors. The implication is that electrophysiology can be used to investigate state

changes in expressed visual pigments. In the expression system the kinetic R_2 relaxation of normal human rhodopsin suggested a minimum of two to three unique charge states. R_2 relaxation can be parametrized to compare electrical states of normal and site-directed mutant visual pigments.

This approach is likely to expand knowledge of structure-function relationships in both rod and cone rhodopsins. Electrophysiology examines state changes along a vector directed *across* the membrane dielectric. Therefore, the expression ERC approach is likely to contribute to mechanistic understanding of conformational and chemical state changes in membrane-oriented visual pigments that are known to have important activation processes directed orthogonal to the membrane plane.

The corresponding author thanks Dr. Paul Sieving (University of Michigan) who provided space in his lab for this project during its early development. We thank Dr. Jeremy Nathans (Johns Hopkins) for providing the WT-HEK293S cell line, Dr. Barry Knox (SUNY) for providing 1D4 resin and access to his spectrophotometer, Dr. Mary Pierce (SUNY) for use of her Hoffman microscope, and Dr. James Schwob (SUNY) for use of his fluorescence microscope. We thank Drs. Maria Giovanni (National Eye Institute) and Rosalie Crouch (Medical University of South Carolina) for providing 11-*cis*-retinal. We thank Dr. Robert Molday for providing permission to use the 1D4 monoclonal rhodopsin antibody. The authors thank Dr. Michael Sheets (Northwestern University) for sharing his recipes and techniques on recording gating currents from fused HEK293 cells, and Dr. Hugh McDowell (University of Florida, Gainesville) for his advice and recipes for FAF-BSA regeneration. The authors thank Dr. Ken Foster (Syracuse University) for carrying out a deconvolution of our action spectra data. The technical assistance of Michael F. Satchwell is acknowledged. We thank Drs. Robert B. Birge, Ken W. Foster, Barry E. Knox, and Edward N. Pugh, Jr. for stimulating scientific discussions. We thank Dr John A. Hoepner (Chair, Dept. of Ophthalmology, SUNY) for encouragement. We appreciate the critical review of the manuscript by Drs. Robert B. Birge, Kenneth W. Foster, Edward N. Pugh, Jr., and Richard D. Veenstra before its submission.

The corresponding author thanks the Foundation Fighting Blindness for their initial sponsorship of this work during a Research Career Development Fellowship (Harry J. Hocks Memorial). In addition, the support of the Heed Foundation (Heed/Knapp Fellowship) is gratefully acknowledged in the early phases of this project. A Hendricks grant and Dept. of Ophthalmology (also supported by Research to Prevent Blindness) startup funds at the SUNY Health Science Center are gratefully acknowledged. Most of this work was supported by an R29 award (EY11384; to J.M.S.) from the National Eye Institute.

REFERENCES

Altenbach, C., K. Yang, D. L. Farrens, Z. T. Farahbakhsh, H. G. Khorana, and W. L. Hubbell. 1996. Structural features and light-dependent changes in the cytoplasmic interhelical E–F loop region of rhodopsin: a site-directed spin-labeling study. *Biochemistry.* 35:12470–12478.

Arden, G. B., C. D. B. Bridges, H. Ikeda, and I. M. Siegel. 1968. Mode of generation of the early receptor potential. *Vision Res.* 8:3–24.

Arnis, S., K. Fahmy, K. P. Hofmann, and T. P. Sakmar. 1994. A conserved carboxylic acid group mediates light-dependent proton uptake and signaling by rhodopsin. *J. Biol. Chem.* 269:23879–23881.

Arnis, S., and K. P. Hofmann. 1993. Two different forms of metarhodopsin II: Schiff base deprotonation precedes proton uptake and signaling state. *Proc. Natl. Acad. Sci. USA.* 90:7849–7853.

Baldwin, J. M. 1993. The probable arrangement of the helices in G protein-coupled receptors. *EMBO J.* 12:1693–1703.

Bennett, N. 1980a. Optical study of the light-induced protonation changes associated with the metarhodopsin II intermediate in rod-outer-segment membranes. *Eur. J. Biochem.* 111:99–103.

Bennett, N. 1980b. Cyanine dye measurement of a light-induced transient membrane potential associated with the metarhodopsin II intermediate in rod-outer-segment membranes. *Eur. J. Biochem.* 111:105–109.

Bezanilla, F., and E. Stefani. 1994. Voltage-dependent gating of ionic channels. *Annu. Rev. Biophys. Biomol. Struct.* 23:819–846.

Birge, R. R., C. M. Einterz, H. M. Knapp, and L. P. Murray. 1988. The nature of the primary photochemical events in rhodopsin and isorhodopsin. *Biophys. J.* 53:367–385.

Bownds, D. 1967. Site of attachment of retinal in rhodopsin. *Nature*. 216:1178–1181.

Cafiso, D. S., and W. L. Hubbell. 1980. Light-induced interfacial potentials in photoreceptor membranes. *Biophys. J.* 30:243–264.

Cone, R. A. 1967. Early receptor potential: photoreversible charge displacement in rhodopsin. *Science*. 155:1128–1131.

Cone, R. A., and W. L. Pak. 1971. The early receptor potential. *In* Handbook of Sensory Physiology: Principles of Receptor Physiology, Vol. 1. W. R. Lowenstein, editor. Springer-Verlag, Berlin. 345–365.

Corey, D. P., and C. F. Stevens. 1983. Science and technology of patch-recording electrodes. *In* Single Channel Recording. B. Sakmann and E. Neher, editors. Plenum Press Inc., New York. 53–68.

Dilley, R. A., and D. G. McConnell. 1970. Alpha-tocopherol in the retinal outer segment of bovine eyes. *J. Membr. Biol.* 2:317–323.

Drachev, L. A., G. R. Kalamkarov, A. D. Kaulen, M. A. Ostrovsky, and V. P. Skulachev. 1981. Fast stages of photoelectric processes in biological membranes. II. Visual rhodopsin. *Eur. J. Biochem.* 117:471–481.

Ebrey, T. G. 1968. The thermal decay of the intermediates of rhodopsin in situ. *Vision Res.* 8:965–982.

Fahmy, K., F. Jager, M. Beck, T. A. Zvyaga, T. P. Sakmar, and F. Siebert. 1993. Protonation states of membrane-embedded carboxylic acid groups in rhodopsin and metarhodopsin II: a Fourier-transform infrared spectroscopy study of site-directed mutants. *Proc. Natl. Acad. Sci. USA.* 90:10206–10210.

Fahmy, K., and T. P. Sakmar. 1993. Regulation of the rhodopsin-transducin interaction by a highly conserved carboxylic acid group. *Biochemistry*. 32:7229–7236.

Farahbakhsh, Z. T., K. Hideg, and W. L. Hubbell. 1993. Photoactivated conformational changes in rhodopsin: a time-resolved spin label study. *Nature*. 262:1416–1419.

Farahbakhsh, Z. T., K. D. Ridge, H. G. Khorana, and W. L. Hubbell. 1995. Mapping light-dependent structural changes in the cytoplasmic loop connecting helices C and D in rhodopsin: a site-directed spin labeling study. *Biochemistry*. 34:8812–8819.

Ganter, U. M., W. Gartner, and F. Siebert. 1988. Rhodopsin-lumirhodopsin phototransition of bovine rhodopsin investigated by Fourier transform infrared difference spectroscopy. *Biochemistry*. 27:7480–7488.

Ganter, U. M., E. D. Schmid, D. Perez-Sala, R. R. Rando, and F. Siebert. 1989. Removal of the 9-methyl group of retinal inhibits signal transduction in the visual process. A Fourier transform infrared and biochemical investigation. *Biochemistry*. 28:5954–5962.

Govardovskii, V. I. 1979. Mechanism of the generation of the early receptor potential and an electrical model of the rod of the intact rat retina. *Biophysics*. 23:520–526.

Hamill, O. P., A. Marty, E. Neher, B. Sakmann, and F. J. Sigworth. 1981. Improved patch-clamp techniques for high-resolution current recording in cells and cell-free membrane patches. *Pflugers Arch.* 391:85–100.

Han, M., S. W. Lin, M. Minkova, S. O. Smith, and T. P. Sakmar. 1996. Functional interaction of transmembrane helices 3 and 6 in rhodopsin. *J. Biol. Chem.* 271:32337–32342.

Hestrin, S., and J. I. Korenbrot. 1990. Activation kinetics of retinal cones and rods: response to intense flashes of light. *J. Neurosci.* 10: 1967–1973.

Hochstrate, P., M. Lindau, and H. Ruppel. 1982. On the origin and the signal-shaping mechanism of the fast photosignal in the vertebrate retina. *Biophys. J.* 38:53–61.

Hodgkin, A. L., and P. M. O'Bryan. 1977. Internal recording of the early receptor potential in turtle cones. *J. Physiol.* 267:737–766.

Hong, K., and W. L. Hubbell. 1973. Lipid requirements for rhodopsin regenerability. *Biochemistry*. 12:4517–4523.

Honig, B. H., W. L. Hubbell, and R. F. Flewelling. 1986. Electrostatic interactions in membranes and proteins. *Annu. Rev. Biophys. Chem.* 15:163–193.

Jager, F., K. Fahmy, T. P. Sakmar, and F. Siebert. 1994. Identification of glutamic acid 113 as the Schiff base proton acceptor in the metarhodopsin II photointermediate of rhodopsin. *Biochemistry*. 33:10878–10882.

Jager, S., M. Han, J. W. Lewis, I. Szundi, T. P. Sakmar, and D. S. Kliger. 1997. Properties of early photolysis intermediates of rhodopsin are affected by glycine 121 and phenylalanine 261. *Biochemistry*. 36: 11804–11810.

Jones, G. J., R. K. Crouch, B. Wiggert, M. C. Cornwall, and G. J. Chader. 1989. Retinoid requirements for recovery of sensitivity after visual pigment bleaching in isolated photoreceptors. *Proc. Natl. Acad. Sci. USA*. 86:9606–9610.

Kersting, U., H. Joha, W. Steigner, B. Gassner, G. Gstaunthaler, W. Pfaller, and H. Oberleithner. 1989. Fusion of cultured dog kidney (MDCK) cells. I. Technique, fate of plasma membranes and of cell nuclei. *J. Membr. Biol.* 111:37–48.

Kibelbek, J., D. C. Mitchell, J. M. Beach, and B. J. Litman. 1991. Functional equivalence of metarhodopsin II and the G_t-activating form of photolyzed bovine rhodopsin. *Biochemistry*. 30:6761–6768.

Klinger, A. L., and M. S. Braiman. 1992. Structural comparison of metarhodopsin II, meta-rhodopsin III, and opsin based on kinetic analysis of Fourier transform infrared difference spectra. *Biophys. J.* 63:1244–1255.

Knowles, A., and H. J. A. Dartnall. 1977. The photobiology of vision. *In* The Eye. H. Davson, editor. Academic Press, New York.

Konig, B., A. Arendt, J. H. McDowell, M. Kahlert, P. A. Hargrave, and K. P. Hofmann. 1989. Three cytoplasmic loops of rhodopsin interact with transducin. *Proc. Natl. Acad. Sci. USA*. 86:6878–6882.

Lamola, A. A., T. Yamane, and A. Zipp. 1974. Effect of detergents and high pressure upon the metarhodopsin I⇔metarhodopsin II equilibrium. *Biochemistry*. 13:738–745.

Lewis, J. W., C. M. Einterz, S. J. Hug, and D. S. Kliger. 1989. Transition dipole orientations in the early photolysis intermediates of rhodopsin. *Biophys. J.* 56:1101–1111.

Lewis, J. W., and D. S. Kliger. 1992. Photointermediates of visual pigments. *J. Bioenerg. Biomembr.* 24:201–210.

Liebman, P. A., W. S. Jagger, M. W. Kaplan, and F. G. Bargroot. 1974. Membrane structure changes in rod outer segments associated with rhodopsin bleaching. *Nature*. 251:31–36.

Lindau, M., and H. Ruppel. 1983. Evidence for conformational substates of rhodopsin from kinetics of light-induced charge displacement. *Photobiochem. Photobiophys.* 5:219–228.

Lindau, M., and H. Ruppel. 1985. On the nature of the fast light-induced charge displacement in vertebrate photoreceptors. *Photobiochem. Photobiophys.* 9:43–56.

Lisman, J. E., and H. Behring. 1977. Electrophysiological measurement of the number of rhodopsin molecules in single *Limulus* photoreceptors. *J. Gen. Physiol.* 70:621–633.

Longstaff, C., R. Calhoon, and R. R. Rando. 1986. Deprotonation of the Schiff base of rhodopsin is obligatory in the activation of the G protein. *Proc. Natl. Acad. Sci. USA*. 83:4209–4213.

MacNichol, E. F. 1978. A photon counting microspectrophotometer for the study of single vertebrate photoreceptor cells. *In* Frontiers of Visual Science. J. S. Cool and E. L. Smith, editors. Springer-Verlag, New York. 194–208.

Makino, C. L., W. R. Taylor, and D. A. Baylor. 1991. Rapid charge movements and photosensitivity of visual pigments in salamander rods and cones. *J. Physiol.* 442:761–780.

Margolskee, R. F., B. McHendry-Rinde, and R. Horn. 1993. Panning transfected cells for electophysiological studies. *BioTechniques*. 15: 906–911.

Marty, A., and E. Neher. 1983. Tight-seal whole-cell recording. *In* Single Channel Recording. B. Sakmann and E. Neher, editors. Plenum Press, New York. 107–122.

McDowell, J. H. 1993. Preparing rod outer segment membranes, regenerating rhodopsin, and determining rhodopsin concentration. *Methods Neurosci.* 15:123–130.

Misra, S. 1998. Contribution of proton release to the B2 photocurrent of bacteriorhodopsin. *Biophys. J.* 75:382–388.

Miyaguchi, K., C.-H. Kuo, and P. H. Hashimoto. 1992. Topography of opsin within disk and plasma membranes revealed by a rapid-freeze deep-etch technique. *J. Neurocytol.* 21:807–819.

Molday, R. S., and D. MacKenzie. 1983. Monoclonal antibodies to rhodopsin: characterization, cross-reactivity, and application as structural probes. *Biochemistry*. 22:653–660.

Moltke, S., M. P. Heyn, M. P. Krebs, R. Mollaaghababa, and H. G. Khorana. 1992. Low pH photovoltage kinetics of bacteriorhodopsin with replacements of Asp-96, -85, -212 and Arg-82. *In* Structures and Functions of Retinal Proteins, Vol. 221. J. L. Rigaud, editor. Colloque INSERM, John Libbey Eurotext Ltd, Versailles, France, 201–204.

Nathans, J. 1990a. Determinants of visual pigment absorbance: role of charged amino acids in the putative transmembrane segments. *Biochemistry*. 29:937–942.

Nathans, J. 1990b. Determination of visual pigments absorbance: identification of the retinylidene Schiff base counterion in bovine rhodopsin. *Biochemistry*. 29:9746–9752.

Nathans, J., C. J. Weitz, N. Agarwal, I. Nir, and D. S. Papermaster. 1989. Production of bovine rhodopsin by mammalian cell lines expressing cloned cDNA: spectrophotometry and subcellular localization. *Vision Res.* 29:907–914.

Oprian, D. D. 1993. Expression of opsin genes in COS cells. *Methods Neurosci.* 15:301–306.

Ostroy, S. E. 1974. Hydrogen ion changes of rhodopsin. pK changes and the thermal decay of metarhodopsin II_{380}. *Arch. Biochem. Biophys.* 164:275–284.

Parkes, J. H., and P. A. Liebman. 1984. Temperature and pH dependence of the metarhodopsin I-metarhodopsin II kinetics and equilibria in bovine rod disk membrane suspensions. *Biochemistry*. 23:5054–5061.

Pugh, E. N., Jr. 1975. Rhodopsin flash photolysis in man. *J. Physiol.* 248:393–412.

Rae, J. L., and R. A. Levis. 1984. Patch voltage clamp of lens epithelial cells: theory and practice. *Mol. Physiol.* 6:115–162.

Rath, P., L. L. J. deCaluwe, P. H. M. Bovee-Geurts, W. J. deGrip, and K. J. Rothschild. 1993. Fourier transform infrared difference spectroscopy of rhodopsin mutants: light activation of rhodopsin causes hydrogen-bonding change in residue aspartic acid-83 during Meta II formation. *Biochemistry*. 32:10277–10282.

Rothschild, K. J., and W. J. deGrip. 1986. FTIR studies of rhodopsin transduction mechanism. *Photobiochem. Photobiophys.* 13:245–258.

Sakmar, T. P., R. R. Franke, and H. G. Khorana. 1989. Glutamic acid 113 serves as the retinylidene Schiff base counterion in bovine rhodopsin. *Proc. Natl. Acad. Sci. USA*. 86:8309–8313.

Sengbusch, G. V., and H. Stieve. 1971. Flash photolysis of rhodopsin. I. Measurements on bovine rod outer segments. *Z. Naturforschung*. 26B: 488–489.

Sheets, M. F., J. W. Kyle, S. Krueger, and D. A. Hanck. 1996. Optimization of a mammalian expression system for the measurement of sodium channel gating currents. *Am. J. Physiol.* 271:C1001–C1006.

Shieh, T., M. Han, T. P. Sakmar, and S. O. Smith. 1997. The steric trigger in rhodopsin activation. *J. Mol. Biol.* 269:373–384.

Simmeth, R., and G. W. Rayfield. 1990. Evidence that the photoelectric response of bacteriorhodopsin occurs in less than 5 picoseconds. *Biophys. J.* 57:1099–1101.

Spalink, J. D., and H. Stieve. 1980. Direct correlation between the R2 component of the early receptor potential and the formation of metarhodopsin II in the excised bovine retina. *Biophys. Struct. Mech.* 6:171–174.

Sullivan, J. M. 1996. Rhodopsin early receptor currents following flash photolysis of single cells expressing human rhodopsin. *Invest. Ophthal. Vis. Sci.* 37:S811.

Sullivan, J. M. 1998. Low-cost monochromatic microsecond flash microbeam apparatus for single-cell photolysis of rhodopsin or other photolabile pigments. *Rev. Sci. Instrum.* 69:527–539.

Sullivan, J. M., and M. F. Satchwell. 1999. Development of stable cell lines expressing high levels of point mutants of human opsin for biochemical and biophysical studies. *Methods Enzymol.* In press.

Sung, C.-H., B. G. Schneider, N. Agarwal, D. S. Papermaster, and J. Nathans. 1991. Functional heterogeneity of mutant rhodopsins responsible for autosomal dominant retinitis pigmentosa. *Proc. Natl. Acad. Sci. USA.* 88:8840–8844.

Szuts, E. Z., and F. I. Harosi. 1991. Solubility of retinoids in water. *Arch. Biochem. Biophys.* 287:297–304.

Thorgeirsson, T. E., J. W. Lewis, S. E. Wallace-Williams, and D. S. Kliger. 1993. Effects of temperature on rhodopsin photointermediates from lumirhodopsin to metarhodopsin II. *Biochemistry*. 32:13861–13872.

Trissl, H. W. 1982a. On the rise time of the R1-component of the "early receptor potential": evidence for a fast light-induced charge separation in rhodopsin. *Biophys. Struct. Mech.* 8:213–230.

Trissl, H. W. 1982b. Electrical responses to light: fast photovoltages of rhodopsin-containing membrane systems and their correlation with the spectral intermediates. *Methods Enzymol.* 81:431–439.

Trissl, H. W., and W. Gartner. 1987. Rapid charge separation and bathochromic absorption shift of flash-excited bacteriorhodopsins containing 13-cis or all-trans forms of substituted retinals. *Biochemistry*. 26: 751–758.

Wald, G., and P. K. Brown. 1958. Human rhodopsin. *Science*. 127:22–226.

Weitz, C. J., and J. Nathans. 1992. Histidine residues regulate the transition of photoexcited rhodopsin to its active conformation, metarhodopsin II. *Neuron*. 8:465–472.

Weitz, C. J., and J. Nathans. 1993. Rhodopsin activation: effects on the metarhodopsin I-metarhodopsin II equilibrium of neutralization or introduction of charged amino acids within putative transmembrane segments. *Biochemistry*. 32:14176–14182.

Williams, T. P. 1964. Photoreversal of rhodopsin bleaching. *J. Gen. Physiol.* 47:679–689.

Williams, T. P. 1965. Rhodopsin bleaching: relative effectiveness of high and low intensity flashes. *Vision Res.* 5:633–638.

Zhukovsky, E. A., and D. D. Oprian. 1989. Effect of carboxylic acid side chains on the absorption maximum of visual pigments. *Science*. 246: 928–930.

Zylka, M. J., and B. J. Schnapp. 1996. Optimized filter set and viewing conditions for the S65T mutant of GFP in living cells. *BioTechniques*. 21:220–226.